Title

A crossed molecular beam investigation of the reaction Cl + propane {yields} HCl + C{sub 3}H{sub 7} using VUV synchrotron radiation as a product probe

Journal

Chemical Physics, 231(2/3/2008)

Author

Blank, David A.

Publication Date

1997-10-20

LBNL-40947
UC-401
Preprint

ERNEST ORLANDO LAWRENCE
BERKELEY NATIONAL LABORATORY

A Crossed Molecular Beam Investigation of the Reaction Cl + Propane → HCl + C_3H_7 Using VUV Synchrotron Radiation as a Product Probe

David A. Blank, Naoki Hemmi,
Arthur G. Suits, and Yuan T. Lee

Chemical Sciences Division

October 1997

Submitted to
Chemical Physics

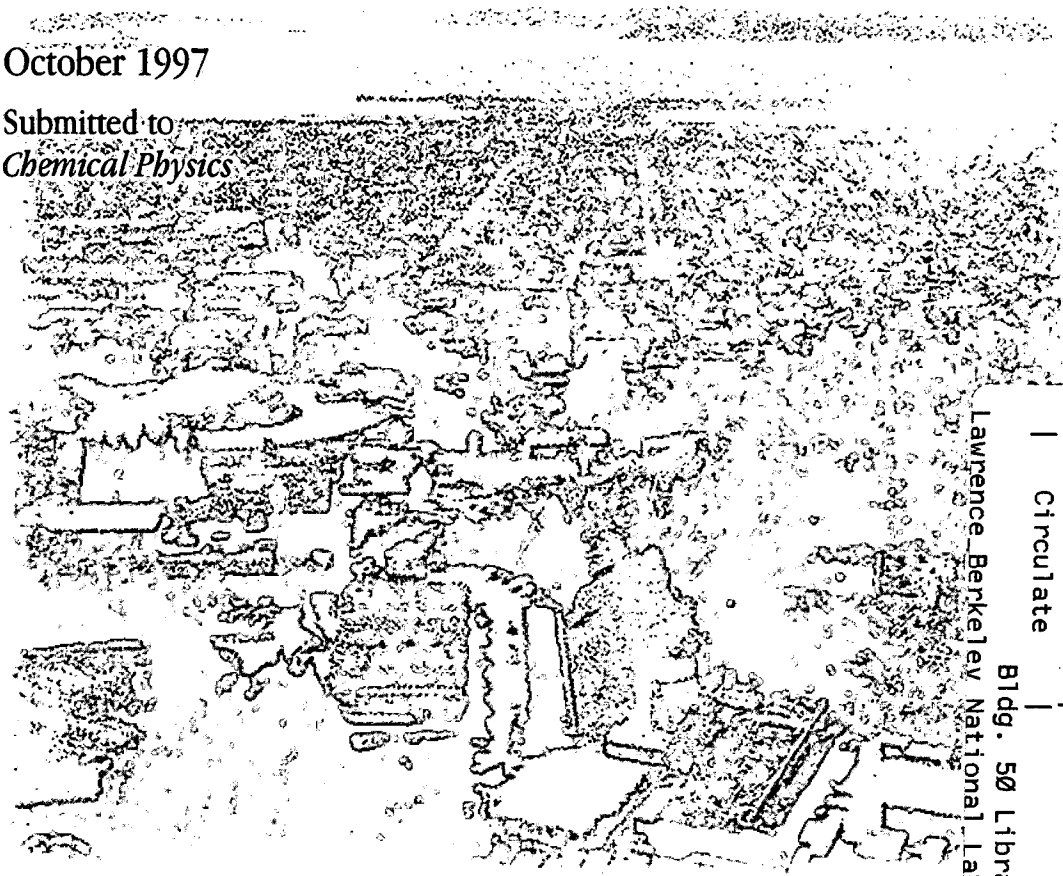

DISCLAIMER

LBNL-40947
UC-401

A Crossed Molecular Beam Investigation of the Reaction Cl + Propane → HCl + C_3H_7 Using VUV Synchrotron Radiation as a Product Probe

David A. Blank, Naoki Hemmi, Arthur G. Suits, and Yuan T. Lee

Chemical Sciences Division
Ernest Orlando Lawrence Berkeley National Laboratory
University of California
Berkeley, California 94720

October 1997

This work was supported by the Director, Office of Energy Research, Office of Basic Energy Sciences, Chemical Sciences Division, of the U.S. Department of Energy under Contract No. DE-AC03-76SF00098.

A crossed molecular beam investigation of the reaction Cl + propane → HCl + C_3H_7 using VUV synchrotron radiation as a product probe

David A. Blank, Naoki Hemmi, Arthur G. Suits, and Yuan T. Lee
Chemical Sciences Division, Lawrence Berkeley Laboratory, University of California, and Chemistry Department, University of California, Berkeley, CA, 94720

Abstract

We have used the crossed molecular beam technique to study the hydrogen atom abstraction from propane by atomic chlorine over a wide range of collision energies. The experiments were carried out using a recently constructed crossed molecular beam apparatus that utilizes tunable VUV synchrotron radiation for product photoionization. We have measured laboratory TOF spectra and angular distributions for E_{coll} = 8.0, 11.5, and 31.6 kcal/mol. Center-of-mass flux maps were generated from the measured laboratory distributions. The results demonstrate two distinct reaction mechanisms that depend on the impact parameter of the reactive collision. Large impact parameter collisions proceed *via* a stripping mechanism resulting in forward scattered products with very little momentum change in going from reactant to product. The stripping reactions are most likely dominated by abstraction of secondary hydrogen atoms. Smaller impact parameter collisions lead to direct reactions with an impulsive recoil and are consistent with a preference for a collinear transition state geometry, -C-H-Cl. The larger energy along the line of centers in smaller impact parameter collisions most likely makes the effect of a larger barrier to abstraction of primary hydrogen atoms negligible leaving the ratio of primary to secondary hydrogen abstraction to be dictated by simple statistics.

1. Introduction

Hydrogen atom abstraction from saturated hydrocarbons by free radicals are reactions of great importance in both atmospheric and combustion chemistry. While there is a wealth of available kinetic information about this class of reactions, by comparison studies investigating the detailed dynamics of these systems are considerably less abundant.

Using molecular beam methods and laser induced flourescence (LIF), Andresen and Luntz measured the internal state distributions of the OH products from the reaction of $O(^3P)$ with a number of alkanes.[1] The alkanes were chosen to provide a comparison between abstraction of a primary [RCH_2-H, *ex.* $C(CH_3)_4$], secondary [R_2CH-H, *ex.* c-C_6H_{12}], or tertiary [R_3C-H, *ex.* $(CH_3)_3CH$] hydrogen atoms. The authors reported only ~2% of the available energy was partitioned into rotation in the OH products. The abstraction of the different types of H atoms resulted in very little change in the rotational distributions. This was interpreted as being indicative of a collinear intermediate configuration (R-H-O) for abstraction of all three types of H atoms. There was only slight broadening of the rotational distributions over a range of collision energies demonstrating the narrow cone of acceptance for reaction about the collinear geometry. Unlike the rotational distributions, the OH(v=1/v=0) population ratios showed a clear dependence on the type of H atom abstracted. Abstraction of primary hydrogen atoms almost exclusively produced OH(v=0) while secondary H atoms resulted in ~25% of the OH products in v=1 and abstraction of tertiary H atom produced slightly more OH(v=1) than OH(v=0). The difference in the vibrational distributions was attributed to the difference in energetics for abstraction of different hydrogen atoms. The exothermicity of the reactions increases from –2.3 kcal/mol for primary H atoms to -7.0 kcal/mol for secondary H atoms and –10.3 kcal/mol for tertiary H atoms. The activation energies increase in the order tertiary <secondary<primary. The argument invoked was that in the less exothermic primary H atom abstraction, which has a larger activation barrier, the transition state geometry should be more product like leading to less vibrational excitation. As the reaction becomes more exothermic with a lower activation energy, primary>secondary>tertiary, the transition state becomes more reactant like and the result is greater product

vibrational excitation. The authors produced good agreement with the experimental results using quasiclassical trajectory calculations assuming a triatomic model for the reaction, R-H-O.[2] The agreement demonstrated the validity of treating the hydrocarbon radical, R, as a structureless particle in these abstraction reactions with the dynamics being dominated by the interaction between the $O(^3P)$ atom and the reactive C-H bond.

Recently, hydrogen atom abstraction from small alkanes by atomic chlorine has been investigated in detail under single collision conditions using resonance enhanced multiphoton ionization (REMPI) of the HCl products and core extracted ion time of flight (TOF) methods. These experiments take advantage of the anisotropic distribution of Cl photoframents in the photodissociation of Cl_2 to generate Cl reactants with a well known velocity and angular distribution. The REMPI ionization of HCl provides nascent rovibrational product state distributions and analysis of the core extracted ion TOF profiles leads to laboratory velocity distributions. Making assumptions about the c.m. speed distribution, c.m. angular distributions can be obtained. These methods have been used by Zare and coworkers and Dagdigian and coworkers to measure state selected differential cross sections for HCl products in the reactions of Cl with a number of saturated hydrocarbons from methane to isobutane.[3,4,5,6,7,8]

The reaction of Cl with methane in its ground vibrational state is slightly endothermic with an activation energy ~2-3 kcal/mol. At a collision energy of 3.7 kcal/mol HCl(v=1) is not thermodynamically accessible and the HCl(v=0) rotational population was found to be very cold.[3] The HCl products were scattered exclusively in the backward direction with respect to the relative velocity of the Cl reactant. Using a hard sphere model, strongly back-scattered products are correlated with small impact parameter (b) collisions. The backward scattering can be intuitively explained within the line-of-centers model[9] where only the collisions at small b lead to sufficient energy along the reaction coordinate to overcome the barrier to reaction. Very low rotational excitation and the strong backward scattering indicate that the transition state for reaction is tightly constrained about a linear geometry, H_3C-H-Cl, analogous to the abstraction reactions of $O(^3P)$ mentioned above.

At the same collision energy, vibrational excitation of the methane reactant, v_3=1, leads to a significant change in the reaction dynamics and a substantial enhancement in the total reactive cross-section.[4] The additional available energy provided by excitation of the methane reactant makes the reaction to produce HCl(v=0,J) exothermic by ~7 kcal/mol and opens up the HCl(v=1,J) product channel which is endothermic by ~2 kcal/mol. The HCl(v=0,J) products are backward scattered in analogy to the reaction with methane in its ground vibrational state, however the HCl(v=0,J) products from the reaction with $CH_4(v_3=1)$ show greater rotational excitation. This was interpreted as demonstrating a similar reaction mechanism in both cases with the additional energy in the methane reactant allowing some degree of relaxation from the strict collinear intermediate geometry. The reactant vibrational energy provides some available energy along the reaction coordinate lessening the energy that must be provided from relative translation and increasing the range of b for reactive collisions. The HCl(v=1,J) products were found to have lower rotational excitation than the HCl(v=0,J) products and exhibited very different scattering. For low J HCl(v=1,J) products the scattering was strongly in the forward direction exhibiting a stripping type mechanism with reactions resulting from large b collisions. With increasing J in the HCl(v=1,J) products, the scattering begins to exhibit an additional component in the backwards direction. The backwards scattering becomes comparable to the component in the forward direction for HCl(v=1, J=3). Lower rotational excitation in the forward scattered products is consistent with the relatively weak interaction experienced in a large b stripping reaction where the CH_3 acts as a spectator. The more backward scattered HCl(v=1,J) products have a slight increase in rotational excitation generated by recoiling with more effective momentum coupling in a smaller b collision providing an additional torque on the departing HCl product.

The reaction of Cl with C_2H_6 is slightly endothermic by ~2 kcal/mol and the authors again found only a small fraction (2%) of the available energy partitioned into HCl product rotation. Their analysis also determined that there was very little internal excitation in the ethyl radical product. While these results were consistent with a developing picture of H atom abstraction that involved a direct reaction with a collinear

intermediate reaction geometry, a nearly isotropic product angular distribution was seemingly at odds with the previous results for the Cl + CH_4 system. The authors explained the difference in the scattering as a result of the greatly reduced reaction barrier in the C_2H_6 reaction. The substantially lower barrier to reaction means that very little of the total translational energy is required along the reaction coordinate in order to produce a reactive collision. Therefore, the restriction on b for reactive collisions between Cl and CH_4(v=0), which comes from the necessity to provide enough energy along the reaction coordinate to overcome the barrier, is almost completely relaxed for ethane. This allows almost every collision between Cl and C_2H_6 to lead to a reaction. The result is a nearly isotropic product angular distribution that is still consistent with the proposed direct reaction mechanism leading to very little internal excitation of the products.

Using the same technique, in addition to the reaction of Cl with methane, Varley and Dagdigian have extended their studies to include larger hydrocarbons investigating the reactions of Cl with propane and isobutane.[6-8] Collision energies were 7.4 kcal/mol and 8.1 kcal/mol respectively. The larger hydrocarbons are complicated by the addition of secondary, in the case of propane, and tertiary, in the case of isobutane, H atoms that compete for abstraction. Abstractions of all three types of H atoms are exothermic with the exothermicity increasing primary<secondary<tertiary. Using isotopically labeled reactants the authors were able to separate abstraction of the different H atoms. Both secondary and tertiary H-atoms, from propane and isobutane respectively, were abstracted preferentially as compared with the neighboring primary H atoms. This result was noted previously for propane by Yen *et al.*[10] The HCl/DCl rotational distributions were found to be cold, in agreement with the previous hydrocarbons studied, again indicating a linear intermediate geometry. Abstraction of the primary hydrogen atoms in both molecules led to mostly backward scattered products, while secondary and tertiary H atom abstraction produced more isotropic and sideways scattered products respectively. In addition, slightly higher rotational excitation of the HCl/DCl products resulted from abstraction of secondary or tertiary H atoms compared with primary H atoms. The greater reactivity, slightly higher rotational excitation of the products, and more isotropic scattering reflects a larger acceptance about the collinear intermediate

geometry that can lead to a reactive collision. Reactions over a large range of b are consistent with the very low activation barriers reported for both of these reactions from kinetic studies.[11] The greater propensity for backwards scattering and the slightly lower rotational excitation in the HCl/DCl products from abstraction of primary H atoms may also suggest a slightly higher barrier to reaction compared with the negligible barrier for abstraction of secondary or tertiary H atoms.

In this study we report the first crossed molecular beam investigation of chemical reaction dynamics using tunable VUV synchrotron radiation to probe the scattered reaction products. We have investigated the hydrogen abstraction reaction from propane by atomic chlorine ($Cl,^2P_{3/2}$) for collision energies ranging from 8.0 kcal/mol to 31.6 kcal/mol. As mentioned above there are two different possible reactions depending on whether a primary or secondary hydrogen atom is abstracted, reactions 1 and 2.[11]

$$C_3H_8 + Cl\ (^2P_{3/2}) \rightarrow HCl + n\text{-}C_3H_7 \qquad \Delta H_o = -2.0\ \text{kcal/mol} \qquad \text{(rxn 1)}$$

$$C_3H_8 + Cl\ (^2P_{3/2}) \rightarrow HCl + i\text{-}C_3H_7 \qquad \Delta H_o = -4.2\ \text{kcal/mol} \qquad \text{(rxn 2)}$$

The rate constant for this reaction has been reported at $(1.2\text{-}1.4)\times10^{-10}$ cm^3 $molecules^{-1}$ s^{-1}, and the temperature dependence over a range 220-600 K produced a very small activation energy of 40 K.[11]

The crossed molecular beam technique using "universal" detection, electron impact ionization of the scattered reaction products followed by a quadrupole mass filter and Daly ion counter, has proven to be one of the most powerful tools in obtaining an complete picture of bimolecular reaction dynamics under single collision conditions for an extensive list of chemical reactions.[12,13] However, the hydrogen atom abstraction reaction provides a particular challenge to this technique. Crossed molecular beam reactive scattering experiments generate an extremely small number density of products at the detection region placing a premium on detection sensitivity for the reaction products. Discriminating against the large background from scattered reactant ^{35}Cl and ^{37}Cl when attempting to detect the signal from HCl products requires very high mass resolution. Very high mass resolution is associated with very low quadrupole

transmission thus greatly reducing the product signal. There is also background from HCl contamination in the Cl beam. Detection of the C_3H_7 product is even more problematic since the scattered C_3H_8 reactant will dissociatively ionize to $C_3H_7^+$ (as well as all $C_{n\leq3}H_{n\leq8}^+$) in the electron bombardment ionizer generating tremendous background that cannot be avoided with mass filtering. Using tunable VUV synchrotron radiation for photoionization of the product molecules in place of electron bombardment provides a solution to these problems. Tuning the VUV photoionization light to an energy above the ionization potential (IP) of the two C_3H_7 isomers but below the IP for the propane provides discrimination against any background generated from dissociative ionization of scattered propane reactants and allows detection of the C_3H_7 products with near background free conditions. In addition, the selective ionization also relaxes the need for mass discrimination between the scattered C_3H_8 reactants appearing at their parent mass, $C_3H_8^+$, and C_3H_7 products allowing much greater quadrupole transmission and thus increased product signal. This selectivity is provided without any spectroscopic knowledge about the products since this is a state independent single photon ionization of the products.

We have measured state average translational energy and angular distributions from the reaction of Cl + propane for collision energies ranging from 8.0 kcal/mol to 31.6 kcal/mol. At the lower collision energy we find a nearly isotropic scattering of the products. The forward scattered products show a larger translational energy release than the backward scattered products. This difference becomes more pronounced with increasing collision energy and there appears to be the emergence of two distinct scattering components at the higher collision energies. These experiments represent the first application of VUV synchrotron radiation for product photoionization in a crossed molecular beam reactive scattering experiment and they demonstrate the power and promise of this new technique for investigations of reactive collisions.

2. Experimental

The experiments were carried out at the Chemical Dynamics Beamline at the Advanced Light Source (ALS) at Lawrence Berkeley National Laboratory. A complete description of the crossed molecular beam apparatus can be found in reference 14. The instrument is based on a previously constructed apparatus that is described in detail elsewhere[15] with the most significant difference being the use of tunable VUV undulator radiation from the ALS for product photoionization in place of electron impact. The continuous propane beam was generated by expanding propane diluted in rare gas through a 0.25 mm stainless steel nozzle. Mixtures of 7% propane in He and 16% propane in He were used. The total stagnation pressure was typically 150 torr and the nozzle was fitted with a resistive heater and K-type thermocouple to allow heating up to 400 °C. The beam was skimmed once with a 0.5 mm stainless steel skimmer and the resulting beam had a full width at half maximum (FWHM) angular divergence of 0.7°.
The continuous molecular beam of atomic chlorine was generated by thermal dissociation of Cl_2 diluted in rare gas mixtures. Mixtures of 2% Cl_2 in He, 7% Cl_2:18% Ar:75% He, and 7% Cl_2 in Ar were used. The typical total stagnation pressure was 600 torr. The pyrolytic molecular beam source is shown in figure 1. The source consists of a high density graphite nozzle with a 0.15 mm opening that is spring loaded into a resistively heated silicon carbide (SiC) front plate. From the rear water cooled copper clamp to within 2 cm of the SiC heating element the wall of the graphite nozzle was 0.5 mm thick in order to reduce conduction of heat between the front and rear of the assembly. A ¼" teflon line was attached to the rear of the graphite nozzle using a hand tightened cajon connection with a rubber O-ring seal for delivery of the Cl_2/rare gas mixture.

The top of figure 2 shows the integrated on axis signal for $^{35}Cl_2^+$(m/e 70) and $^{35}Cl^+$(m/e 35) as a function of the nozzle temperature for a mixture of 7% Cl_2 in He. The nozzle temperature was monitored using optical pyrometery and was found to be consistent with velocity analysis of supersonic rare gas beams to ± 75 °C. Under typical experimental conditions the nozzle was run at 1500-1550 °C providing dissociation of a large fraction of the Cl_2 as can be seen in the top of figure 2. Roughly 250 Watts (10 A, 25 V) across the SiC heating element was required to achieve a temperature of 1500°C.

The Cl beam was skimmed twice, first by a water cooled nickel skimmer with a 1.0 mm opening and then again by a second 1.0 mm stainless steel skimmer. The resulting beam had a FWHM angular divergence of 1.0°. At 1500°C a Boltzmann distribution predicts that ~15% of the chlorine atoms will be in the exited spin-oribit state, $Cl(^2P_{1/2})$.With a large percentage of these being relaxed in the supersonic expansion, the majority of the Cl reactants will be in the ground spin-orbit state, $Cl(^2P_{3/2})$.

Periodic monitoring of the relative intensity of the Cl beam was performed using elastic scattering off a neat supersonic molecular beam of neon. A representative time of flight (TOF) spectrum is shown in the bottom of figure 2 for elastically scattered Cl using a mixture of 7% Cl_2 in He and a nozzle temperature of 1500 °C. The TOF spectrum was taken at a scattering angle of 50° with respect to the neon beam and the scattered Cl atoms were photoionized with 14.5 eV undulator radiation. A scattering angle of 50° is beyond the maximum elastic scattering angle for Cl_2, see the insert newton diagram in the bottom of figure 2, allowing monitoring of the atomic Cl beam without interference from dissociative photoionization of Cl_2. The TOF spectrum in figure 2 was accumulated over only 3 minutes of signal averaging using the cross-correlation technique described below for product velocity analysis.

Instrument purity propane and high purity Cl_2 were obtained from Matheson and used without further purification.

The cross-correlation method was used for velocity analysis of the both reactant beams as well as the reactive scattering products.[16] A 17.8 cm diameter cross-correlation wheel with two identical 255-bit pseudorandom sequences of open and closed slots was used in front of the detector entrance to modulate the incident flux. The wheel was spun at 326.8 Hz resulting in a nominal resolution of 6 μsec in the TOF. The neutral flight length from the wheel to the undulator photoionization is 11.9 cm. For velocity analysis of either molecular beam, the beam being analyzed was placed on line with the detector axis, the aperture at the entrance to the detector was set to 0.075 mm, and the photoionization energy was set to 14.5 eV with Ar in the gas filter. The resulting beam parameters are listed in table1 and the most probable collision energies and spread in the collision energies are listed in table 2.

Detection of the scattered C_3H_7 reaction products was accomplished using 9.5 eV photoionization radiation. A complete description of the photoionization radiation can be found in reference 17. The undulator radiation has a near Gaussian energy profile with a FWHM of 2.5% and it is passed through a rare gas filter filled with 30 torr of argon to suppress the higher harmonics in the undulator spectrum.[18] A MgF_2 filter was also used to remove any residual radiation above the MgF_2 transmission cuttoff of ~11.2 eV.[19] The IP for propane is 10.9 eV and the IPs for the two C_3H_7 isomers are 8.1 eV (n-C_3H_7) and 7.5 eV (i-C_3H_7).[20,21] By using a photoionization energy of 9.5 eV there is almost no background from ionization or dissociative ionization of the C_3H_8 reactants. We detect the C_3H_7 products at m/e 43 ($C_3H_7^+$) and the quadrupole is set with a mass resolution of ~1.2 amu FWHM to maximize ion transmission. TOF spectra were recorded for C_3H_7 products at laboratory scattering angles of $-10°$ to $110°$ with respect to the propane beam. Signals were averaged for 1-3 hours at each angle and laboratory angular distributions were obtained by integration of the TOF spectrum for each angle.

3. Results and Analysis

We measured laboratory angular and TOF distributions for C_3H_7 (at m/e 43, $C_3H_7^+$) products at three center of mass (cm) collision energies, E_c = 8.0, 11.5, 31.6 kcal/mol. The experimental conditions for each collision energy are listed in table 2. Newton diagrams for the three collision energies are shown in the bottom of figures 3, 9, and 15 respectively. The circles in the Newton diagrams represent the maximum recoil for C_3H_7 products given the available energy for the more exothermic abstraction channel, reaction 2.

CM angular distributions, $T(\Theta_{cm})$, and translational energy distributions, $P(E_T)$, were generated from the laboratory angular distributions and TOF spectra using the forward convolution technique.[22] The data demonstrated a strong dependence of the $P(E_T)$ on the cm scattering angle. In general, the forward scattered C_3H_7 products involved a much larger translational energy release than the products scattered in the backwards direction. This effect was most apparent at the two higher collision energies.

In practice it is necessary to simplify the forward convolution simulations by assuming that the cm angular distribution and translational energy distributions are completely separable, $I_{cm}(E_T,\Theta_{cm}) = P(E_T)\cdot T(\Theta_{cm})$. In order to obtain satisfactory fits to the experimental data using the forward convolution technique, four separate sets of decoupled $T(\Theta_{cm})$ and $P(E_T)$ were used. The effect of using multiple sets of decoupled $T(\Theta_{cm})$ and $P(E_T)$ is to provide an effective coupling of $T(\Theta_{cm})$ and $P(E_T)$ in the overall forward convolution fit to the data. The measured laboratory angular distributions and the forward convolution fits are shown in figures 3, 9, and 15 for the three different collision energies The TOF spectra and forward convolution fits are shown in figures 4, 10, and 16. The solid lines in figures 4, 10, and 16 are the forward convolution fits to the data.

As a result of only skimming the propane beam only once, there is a minor component in the TOF spectra from reactions of effusive propane reactants. This component is most apparent at a laboratory angle of 110° and at the lowest collision energy. We used the same forward convolution formalism to simulate the reactions of from the effusive propane reactants that was used for simulation of the scattering from the supersonic propane reactants. Since our current forward convolution software was not equipped to simulate an effusive reactant source, the effusive propane beam was modeled as a supersonic beam with a peak velocity of 300 m/s, $\Delta v/v=1.0$, and a FWHM angular divergence of 7.0°. The contributions to the TOF spectra from effusive reactants are shown as the dash-dot-dash lines in figures 4, 10, and 16, and the dashed lines are the summed total of the products from both the supersonic propane reactants (solid line) and the effusive propane reactants. The forward convolution fits to the laboratory angular distributions, the solid lines in figures 3, 9, and 15, are the summed total of contributions from both supersonic and effusive propane reactants. The inexact representation of the effusive propane reactants is the most likely reason behind our inability to obtain a satisfactory fit to the laboratory angular distributions at 110°. It is at this laboratory angle, 110°, where the products from the effusive propane reactants have the greatest relative contribution to the total measured product number density.

The result of the forward convolution analysis is a best fit cm flux distribution, $I_{cm}(\Theta,E_T)$. The best-fit total cm flux and average translational energy release, $\langle E_T \rangle$, are

shown as a function a cm angle in the bottom and top respectively of figures 5, 11, and 17 for the three collision energies. The $P(E_T)$ at three cm angles are shown in figures 6, 12, and 18, and the total cm velocity flux maps are shown in figures 7, 13, and 19 with both 2-D contour maps and 3-D wire plots. A summary of the cm translational energy release at four cm angles is provided in table 3.

At E_{coll}=8.0 kcal/mol the cm angular distribution is isotropic with $<E_T>$ largest in the forward direction, reaching a minimum at Θ_{cm}=90, and increasing toward scattering in the backward direction, figure 5. At E_{coll}=11.5 kcal/mol the scattering is still nearly isotropic with small peaks appearing in the forward direction (Θ_{cm}~10°) and in the sideways direction (Θ_{cm}~100°). The $<E_T>$ is at a maximum in the forward direction and decreases out to Θ_{cm}=90°. From Θ_{cm}=90° to Θ_{cm}=180° $<E_T>$ remains constant, figure 11. The angular distribution at E_{coll}=31.6 kcal/mol has similar features to E_{coll}=11.5 kcal/mol. Comparison of figures 11 and 17 shows the forward scattered component at E_{coll}=31.6 kcal/mol has increased relative to the sideways/backward scattering and demonstrates broadening toward sideways angles. The sideways/backward scattering is nearly unchanged from E_{coll}=11.5 kcal/mol to E_{coll}=31.6 kcal/mol with $<E_T>$ remaining constant from Θ_{cm}=90°-180° and a small peak appearing in the angular distribution at Θ_{cm}~100°. The $P(E_T)$s are similar in shape at all of the collision energies, figures 6, 12, and 18. The $P(E_T)$s are all peak well away from 0 kcal/mol with the maximum probability occurring at higher energies for smaller cm scattering angles. All of the $P(E_T)$s are fairly broad with a FWHM ~25-30% of the available energy.

At the two higher collision energies we are able to separate the products into two scattering components based on the clear difference in translational energy release for the forward scattered products compared with the sideways/backwards scattered products. These two components are most apparent at E_{coll}=31.6 kcal/mol and can be seen in the contour plot at the bottom of figure 19. The separation of these two components is shown by the dashed lines in the angular distributions in figures 11 and 17. The two scattering components are also illustrated with 3-D flux maps in figures 14 and 20 showing the slower sideways/backward component at the bottom, the faster forward scattered component in the middle, and the total flux map at the top.

Photoionization spectrum of the propyl radical reactant products. We also report the photoionization spectrum for the propyl radical between 6.5 eV and 10.0 eV. Figure 8 shows the integrated signal as a function of the PI energy at m/e 43 ($C_3H_7^+$) for a collision energy of 8.0 kcal/mol and a laboratory scattering angle of 10°. The apertures defining the VUV undulator radiation were set at 5x4 mm resulting in an energy resolution of $\Delta E/E$=2.5% FWHM.[17] Taking into account the width of the VUV PI radiation, figure 8 shows a photoionization onset of 7.5±0.3 eV in excellent agreement with the reported value for the IP of 7.5 eV for *i*-C_3H_7.[21] From table 3, the average translation energy release for forward scattered products at E_{coll}=8.0 kcal/mol is ~60% of the 12.2 kcal/mol available energy or ~7.3 kcal/mol. This leaves ~4.9 kcal/mol on average in internal energy of the two products. Varley *et al.* have reported very little internal excitation of the HCl products, ~2% of the available energy, at a similar collision energy of 7.4 kcal/mol. Therefore, the majority of the 4.9 kcal/mol of internal energy must be partitioned into the C_3H_7 products and the photoionization onset in figure 8 represents *i*-C_3H_7 radicals with $\langle E_{int} \rangle$~4.5 kcal/mol. Since it is possible for internal energy to red shift the photoionization onset, our measured PI onset of 7.5±0.3 eV represents an upper limit to the true vertical ionization energy of internally cold *i*-C_3H_7 radicals. While the resolution of our measurement is not high, this does represent a direct measurement of the photoionization onset for an unstable free radical with a known internal energy. We are able to identify the presence of the *i*-C_3H_7 isomer at θ_{lab}=10° based on the photoionization onset and we have demonstrated the ability of this newly constructed crossed molecular beam instrument to measure the photoionization onsets of reactive scattering products at given laboratory scattering angles.

4. Discussion

Based on our measurements we can immediately eliminate the formation of a reaction complex with a lifetime comparable to or longer than its rotational period. Our measured angular distributions do not exhibit the forward/backward symmetry associated

with a long lived complex and there is a strong dependence of $P(E_T)$ on $T(\Theta_{cm})$. The large partitioning of energy into translation is also contradictory to the statistical division of available energy traditionally found in the decomposition of a long lived reaction complex. All of our results are consistent with a direct reaction mechanism in agreement with the conclusions from previous investigations for H atom abstraction from saturated alkanes.[3-8] The transition states have been calculated by Bottoni *et al.* to be collinear (C-H-Cl) for abstraction of both primary and secondary hydrogen atoms from propane by a chlorine atom.[23] A collinear transition state is further supported by the small amount of rotational excitation in the HCl products measured by Varley and Dagdigian, ~2% of the available energy.[7]

Our measurements show very broad scattering at all measured collision energies with greater translational energy release for forward scattered products than sideways/backwards scattered products. At the two higher collision energies the difference in translational energy of the products is most apparent and suggests a separation of the scattering into two distinct reaction mechanisms. This separation is illustrated in figures 14 and 20.

Table 3 shows that the forward scattered products, $\Theta_{cm}=10°$, demonstrate an increase in the fraction of available energy partitioned into translation with an increase in collision energy. As the collision energy is increased, the fraction of the available energy provided by the reaction exothermicity is decreased. In other words, the translational energy release in the forward scattered products appears to scale with the energy of collision and demonstrates very little sensitivity to the energy released in the reaction. The contour maps in figures 7, 13, and 19 show that the forward scattered products have a maximum probability around the cm velocity of the incident propane reactants. With the small change in mass from propane reactant to propyl radical product, the lack of change in velocity reflects almost no change in momentum of the reactants as they pass through the transition state. The forward scattering and the lack of change in momentum of the reactants indicate reactions with large impact parameters and weak interactions at the transition state. These are hallmarks of the spectator/stripping reaction mechanism.

The limited interaction of the reactants in a stripping mechanism is also consistent with the small rotational excitation in the HCl products measured by Varley and Dagdigian.[7]

The large impact parameters translate into a perpendicular approach (perpendicular to the C-H bond of the H atom being abstracted) and very little velocity along the reaction coordinate (C-H-Cl). Therefore, forward scattered products are limited to reactions with barriers that are small compared to the collision energy. Kinetic studies over a range 220-600 K found a very small activation energy of 40 K (~0.1 kcal/mol) consistent with our observed stripping mechanism.[11] This activation energy reflects abstraction of the H atoms with the smallest barrier. In accordance with the weaker C-H bond, *ab initio* calculations found the barrier to abstraction of secondary H atoms, reaction 2, to be lower than the barrier to primary H atom abstraction, reaction 1. Our measured photoionization onset of 7.5±0.3 eV for forward scattered C_3H_7 products, figure 8, is also consistent with production of *i*-C_3H_7 (IP=7.5 eV), reaction 2. From our results is likely that the forward scattering is dominated by reaction 2, particularly at lower collision energies.

As the collision energy is increased, the forward scattering component shows broadening to larger cm angles and an increase in intensity at the highest collision energy with respect to the sideways/backwards scattering, see figures 5, 11, and 17. This could indicate the opening/increase of a stripping mechanism for primary hydrogen atoms, reaction 1. Although the barrier to reaction 1 may only be ~1 kcal/mol above the near absent barrier for reaction 2 (*ab initio* values suggest the barrier could be as much as 4 kcal/mol above the barrier for reaction 2)[11], and our collision energies are 8.0 kcal/mol and above, the increase in forward scattering with collision energy is still consistent with an increase in stripping of primary hydrogen atoms. As mentioned above, the geometry of a stripping reaction leads to very little of the relative reactant translation along the C-H-Cl reaction coordinate. The situation is worse for primary H-atoms compared with secondary H-atoms. A collinear C-H-Cl approach in the case of primary H-atoms has an impact parameter that is ~1.5-2 times that of a collinear approach for secondary H-atoms. This means that the abstraction of a primary H-atom must also overcome a larger centrifugal barrier. With a stripping mechanism providing very little of the relative

translational energy along the C-H-Cl reaction coordinate, we should still observe a limited increase in stripping of primary H-atoms with an increase in collision energy even for collision energies that are large compared to the small reaction barrier.

The sideways/backward scattered component is consistent with recoiling from collisions at smaller impact parameters for reactions favoring a collinear approach, -C-H-Cl. The sideways/backward scattered component demonstrates a consistent partitioning of 50% of the available energy into translation at all three collision energies, see table 3. The strong coupling of internal energy in the products with the available energy is in clear contrast with the stripping seen in the forward direction and reflects the greater coupling of reactant momentum to product rotation in collisions with smaller impact parameters. Our measured translational energy release is consistent with an impulsive product recoil from a direct, exothermic reaction at smaller impact parameters. An impulsive recoil will impart a torque about the cm of the departing fragments with a larger collision energy leading to a larger impulse and greater internal excitation of the products. Initially, the cold HCl rotational distributions measured by Varley and Dagdiagian at a collision energy of 7.4 kcal/mol may appear to contradict an impulsive recoil from small b collisions.[7] However, a preferred collinear -C-H-Cl geometry would leave the impulse of the recoil primarily along the H-Cl bond with limited torque on the HCl product. Therefore, most of the available energy that is not partitioned into translation, 50%, is partitioned into internal energy of the C_3H_7 products. Note that a collinear C-H-Cl reaction geometry will have an impact parameter of ~0.6 Å for reaction 2 and 0.9-1.2 Å for reaction 1 leaving an impulsive recoil to impart a significant torque on the C_3H_7 products, consistent with our observed energy partitioning.[7]

As the collision energy is increased from 8.0 kcal/mol to 11.5 kcal/mol the backward scattering spreads to smaller cm angles and at the higher collision energies a peak in the sideways direction, Θ_{cm}~100°, begins to emerge. We can use the line of centers model which was successfully employed to explain the scattering from Cl + vibrationally cold methane and ethane.[4,5] In this case we refer to the collinear -C-H-Cl coordinate as the line of centers, not the line between the cm of the reactants. As the collision energy is increased, the range of impact parameters that impart sufficient energy

along the reaction coordinate to overcome the reaction barrier is increased leading to a broader scattering distribution. With almost no effective barrier to abstraction of secondary H-atoms, the spreading out of the backward scattering when increasing E_{coll} from 8.0 kcal/mol to 11.5 kcal/mol suggests that a significant fraction of the sideways/backward scattered products are the result of primary H-atom abstraction. Since the impact parameter for sideways/backwards scattering (in a direct reaction) is relatively small, there will be sufficient energy along the line of centers for reaction to occur in almost every collision, especially for the higher collision energies. Therefore, it is likely that abstraction of primary H-atoms will be the more dominant channel based simply on the statistical advantage, outnumbering the secondary H-atoms 3:1. A preferred collinear geometry, C-H-Cl, is also consistent with the peaking at Θ_{cm}~100° for the two higher collision energies. For abstraction of primary H-atoms, a preferred collinear C-H-Cl geometry will have an impact parameter of 0.9-1.2 Å leading to preferred sideways scattering of the products. The broad range of scattering in the sideways/backward directions reflects the large range of impact parameters that lead to reaction.

In addition to measuring the HCl product state distributions Varley and Dagdigian also measured the angular distributions for HCl and DCl products using $CD_3CH_2CD_3$.[7] The DCl products showed sideways/backward scattering in good agreement with our conclusion that primary H-atom abstraction produces sideways/backward scattering, particularly at lower collision energies. The HCl products were more isotropically scattered. This is less consistent with our results. Although the secondary H-atom abstraction should proceed by both of the mechanisms we have observed, our results suggest that the stripping mechanism should be the more dominant mechanism for reaction 2. The Varley and Dagdigian results actually show a drop-off in scattering toward more forward angles. One possible explanation comes from the assumption made by Varley and Dagdigian of zero internal energy in the C_3H_7 product when analyzing the 1-D ion TOF spectra to generate cm angular distributions. The authors mention that increasing the internal energy to 5 kJ/mol had no significant effect on the resulting cm angular distribution. However, our results found 40-50% of the available energy partitioned into internal energy and this partitioning showed a strong dependence on the

scattering angle. With the very small HCl internal energy measured by Varley and Dagdigian most of the internal energy must be in the C_3H_7 products. For their collision energy of 7.4 kcal/mol this corresponds to 3.0-3.7 kcal/mol of internal excitation in the C_3H_7 products or ~3 times the internal energy reported as having a minimal effect on the data analysis leading to the reported angular distributions.

As mentioned above, the sideways/backwards scattering we observe is consistent with the line of centers model used to describe the results of Zare and coworkers for Cl + vibrationally cold methane and ethane.[3-5] The reaction of Cl + CH_4(v=0) produced exclusive backwards scattering since only small b collisions provided sufficient energy along C-H-Cl to overcome the endothermic reaction barrier. In the case of ethane the authors suggested that the sideways/isotropic scattering they observed was the result of a greatly diminished reaction barrier compared with methane allowing nearly every collision to lead to a reaction. The non-zero impact parameter associated with a preferred collinear reaction geometry could also help promote sideways scattering. However, this effect will be much less in Cl + ethane than Cl + propane since a collinear geometry in ethane has an impact parameter of only ~0.17 Å compared with 0.9-1.2 Å for a primary hydrogen in propane. The smaller impact parameter for the preferred geometry in ethane will also lead to significantly less rotational excitation of the ethyl radical product in an impulsive recoil. A smaller internal energy helps avoid the difficulty faced in the data analysis of Varley and Dagdigian for Cl + propane (see paragraph above) when assuming near zero internal energy in the hydrocarbon radical for analysis of the 1-D ion TOF spectra. Hydrogen atom abstraction in ethane should be similar to abstraction of primary H-atoms from propane and the scattering from Cl + ethane is similar to our sideways scattered products that we conclude are predominantly from abstraction of primary H-atoms.

The stripping mechanism we observed is similar to the forward scattering reported from $CH_4(v_3=1)$. The additional vibrational energy in the methane reactant was suggested to significantly lower the barrier to reaction allowing reactions for large b collisions. This is analogous to the smaller barrier for abstraction of secondary H-atoms compared with primary H-atoms in propane. For H-atom abstraction from $CH_4(v_3=1)$ the

forward scattered HCl products were preferentially found in v=1 as a result of efficient coupling between the v_3 vibration in the CH_4 reactants and the HCl products. With vibrationally cold propane reactants we expect the stripping reaction to lead to vibrationally cold HCl products, consistent with the measurements of Varley and Dagdigian.[7]

5. Conclusion

We have used the crossed molecular beam technique to investigate the reaction Cl + propane $\rightarrow$ HCl + C_3H_7 at three collision energies, 8.0, 11.5, and 31.6 kcal/mol. We have observed two distinct reaction mechanisms. Collisions with large impact parameters preferentially abstract a secondary hydrogen atom *via* a spectator/stripping reaction mechanism. There is an increase in the stripping component at the highest collision energy that may suggest stripping of primary hydrogen atoms when the collision energies is sufficiently high. The stripping mechanism is similar to the mechanism reported for forward scattering in the reaction Cl + $CH_4(v_3=1)$, however there have been no previous reports of a stripping mechanism for hydrogen atom abstraction from vibrationally cold saturated hydrocarbons. Collisions with smaller impact parameters involve a direct reaction mechanism with an impulsive product recoil and are consistent with a collinear C-H-Cl transition-state geometry. This channel is most likely dominated by abstraction of primary hydrogen atoms and is consistent with the reaction mechanism proposed for the analogous reactions Cl + $CH_4(v=0)$ and Cl + C_2H_6.

Acknowledgments

This work was supported by the Director, Office of Energy Research, Office of Basic Energy Science, Chemical Sciences Division of the U. S. Department of Energy under contract No. DE-AC03-76SF00098. The experiments were conducted at the

Advanced Light Source, Lawrence Berkeley National Laboratory which is supported by the same source.

Table 1. Experimental beam parameters.

Beam Conditions	Peak Beam Velocity (m/s)	Speed Ratio (v/Δv)
Cl (2% Cl_2 in He)	3121	5.7
Cl (7%Cl_2,18%Ar,75%He)	1852	5.8
Cl (7% Cl_2 in Ar)	1382	7.0
C_3H_8 (7% C_3H_8 in He, nozzle at 270°C)	1931	8.6
C_3H_8 (16% C_3H_8 in He, nozzle at 20°C)	1200	11.0

Table 2. Experimental Conditions (cm collision energies).

Cl peak velocity (m/s)	C_3H_8 peak velocity (m/s)	cm collision energy (kcal/mol)	$\Delta E_{coll}/E_{coll}$
3121	1931	31.6	0.32
1852	1205	11.5	0.30
1382	1220	8.0	0.24

Table 3. Average Translational Energy Release

E_{coll} (kcal/mol)	E_{avail}[(a)] (kcal/mol)	$\langle E_T \rangle / E_{avail}$ for given cm angle				$(\Delta \langle E_T \rangle)_{max}$ (kcal/mol)
		$\Theta_{cm}=10°$	$\Theta_{cm}=50°$	$\Theta_{cm}=100°$	$\Theta_{cm}=160°$	
8.0	12.2	0.62	0.54	0.49	0.53	1.8
11.5	15.7	0.68	0.58	0.52	0.52	2.6
31.6	35.8	0.74	0.69	0.51	0.48	9.3

(a) Available energy for abstraction of the secondary hydrogen atom, reaction 2.

References

[1] P. Andresen and A. C. Luntz, *J. Chem. Phys.* **72**, 5842 (1980).

[2] A. C. Luntz and P. Andresen, *J. Chem. Phys.* **72**, 5851 (1980).

[3] W. R. Simpson, T. P. Rakitzis, S. A. Kandel, T. Lev-On, and R. N. Zare, *J. Phys. Chem.* **100**, 7938 (1996).

[4] W. R. Simpson, T. P. Rakitzis, S. A. Kandel, A. J. Orr-Ewing, and R. N. Zare, *J. Chem. Phys.* **103**, 7313 (1995).

[5] S. A. Kandel, T. P. Rakitzis, T. Lev-On, and R. N. Zare, *J. Chem. Phys.* **105**, 7550 (1996).

[6] D. F. Varley and P. J. Dagdigian, *J. Phys. Chem.* **99**, 9843 (1995).

[7] D. F. Varley and P. J. Dagdigian, *Chem. Phys. Lett.* **255**, 393 (1996).

[8] D. F. Varley and P. J. Dagdigian, *J. Phys. Chem.* **100**, 4365 (1995).

[9] R. D. Levine and R. B. Bernstein, *Molecular Reaction Dynamics and Chemical Reactivity*; Oxford University Press: New York, 1987.

[10] Y. Yen, Z. Wang, B. Xue, and B. Koplitz, *J. Phys. Chem.* **98**, 4 (1994).

[11] R. Atkinson, D. L. Baulch, R. A. Cox, R. F. Hampson, J. A. Kerr, and J. Troe, *J. Phys. Chem. Ref. Data* **21**, 1125 (1992).

[12] Y. T. Lee, J. D. McDonald, P. R. LeBreton and D. R. Hershback, *Rev. Sci Instrum.* **40**, 1402 (1969).

[13] Y. T. Lee, *Science* **236**, 793 (1987).

[14] X. Yang, D. A. Blank, J. Lin, P. A. Heimann, A. M. Wodtke, A. Suits, and Y. T. Lee, Rev. Sci. Instrum., *to be published.*

[15] A. M. Wodtke and Y. T. Lee, J. Phys. Chem. 89, 4744 (1985).

[16] K. Skold, Nucl. *Inst. Methods* **63**, 114 (1968); V. L. Hirshy and J. P. Aldridge, *Rev. Sci. Instrum.* **42**, 381 (1971); G. Comsa, R. David, and b. J. Schumacher, *Rev. Sci. Instrum.* **52**, 789 (1981).

[17] P. A. Heimann, M. Koike, C. W. Hsu, M. Evans, C. Y. Ng, D. A. Blank, A. G. Suits, and Y. T. Lee, *SPIE*, (1996), vol. **2856**, 90; P. A. Heimann, M. Koike, C. W. Hsu, M. Evans, K. T. Lu, C. Y. Ng, A. G. Suits, and Y. T. Lee, *Rev. Sci. Instrum.*, *accepted* May 1997.

[18] A. G. Suits, P. Heimann, X. Yang, M. Evans, C. W. Hsu, K. Lu, A. H. Kung, and Y. T. Lee, *Rev. Sci. Instrum.* **66**, 5405 (1995).

[19] J. A. R. Samson, *Techniques of Vacuum Ultraviolet Spectroscopy*, Wiley, New York, 1967.

[20] Handbook of Chemistry and Physics, D.R. Lide (CRC, Boca Raton, 1995).

[21] J. L Franklin, J. G. Dillard, H. M. Ronstock, J. T. Herron, K. Draxl, and F. H. Field, *Ionization Potentials, Appearance Potentials, and Heats of Formation of Gaseous Positive Ions*, Nat. Stand. Ref. Data Ser., Nat. Bur. Stand. (U.S.), June 1969.

[22] R. J. Buss, Ph.D. Thesis, University of California, Berkeley (1995).

[23] A. Bottoni and G. Poggi, *J. Mol. Struct.* **337**, 161 (1995).

Figure Captions

Figure 1: Schematic drawing of the continuous pyrolytic molecular beam source used for generation of the atomic chlorine beam.

Figure 2: Atomic chlorine beam diagnostics. (Top) Plot of the Cl and Cl_2 on axis intensities as a function of the nozzle temperature. (Bottom) Elastic scattering of the atomic chlorine beam off a neat beam of neon. See the inserted newton diagram.

Figure 3: Laboratory angular distribution for C_3H_7 products and Newton diagram for a collision energy of 8.0 kcal/mol. The solid line is the forward convolution fit and the circles are the data.

Figure 4: TOF spectra for C_3H_7 at 10 laboratory angles for a collision energy of 8.0 kcal/mol. Circles are the data, solid line is the forward convolution fit, dash-dot-dash line is the forward convolution fit for the effusive component (see text) and the dashed line is the total fit to the data.

Figure 5: Average translational energy release (top) and total flux (bottom) as a function of cm angle. Collision energy is 8.0 kcal/mol.

Figure 6: $P(E_T)$ at three cm angles, 10°, 40°, and 120°, for a collision energy of 8.0 kcal/mol.

Figure 7: CM flux map for a collision energy of 8.0 kcal/mol.

Figure 8: Photoionization spectrum for the C_3H_7 product at a laboratory angle of 10° and a collision energy of 8.0 kcal/mol.

Figure 9: Laboratory angular distribution for C_3H_7 products and Newton diagram for a collision energy of 11.5 kcal/mol. The solid line is the forward convolution fit and the circles are the data.

Figure 10: TOF spectra for C_3H_7 at 10 laboratory angles for a collision energy of 11.5 kcal/mol. Circles are the data, solid line is the forward convolution fit, dash-dot-dash line is the forward convolution fit for the effusive component (see text) and the dashed line is the total fit to the data.

Figure 11: Average translational energy release (top) and total flux (bottom) as a function of cm angle. Collision energy is 11.5 kcal/mol.

Figure 12: $P(E_T)$ at three cm angles, 10°, 50°, and 120°, for a collision energy of 11.5 kcal/mol.

Figure 13: CM flux map for a collision energy of 11.5 kcal/mol.

Figure 14: Separation of the two reaction mechanisms for a collision energy of 11.5 kcal/mol shown as 3-D flux maps. Bottom map is the sideways/backward scattered component, middle is the forward scattered stripping component, and the top is the total flux map.

Figure 15: Laboratory angular distribution for C_3H_7 products and Newton diagram for a collision energy of 31.6 kcal/mol. The solid line is the forward convolution fit and the circles are the data.

Figure 16: TOF spectra for C_3H_7 at 10 laboratory angles for a collision energy of 31.6 kcal/mol. Circles are the data, solid line is the forward convolution fit, dash-dot-dash line is the forward convolution fit for the effusive component (see text) and the dashed line is the total fit to the data.

Figure 17: Average translational energy release (top) and total flux (bottom) as a function of cm angle. Collision energy is 31.6 kcal/mol.

Figure 18: $P(E_T)$ at three cm angles, 10°, 50°, and 120°, for a collision energy of 31.6 kcal/mol.

Figure 19: CM flux map for a collision energy of 31.6 kcal/mol.

Figure 20: Separation of the two reaction mechanisms for a collision energy of 31.6 kcal/mol shown as 3-D flux maps. Bottom map is the sideways/backward scattered component, middle is the forward scattered stripping component, and the top is the total flux map.

Continuous Pyrolytic Molecular Beam Source

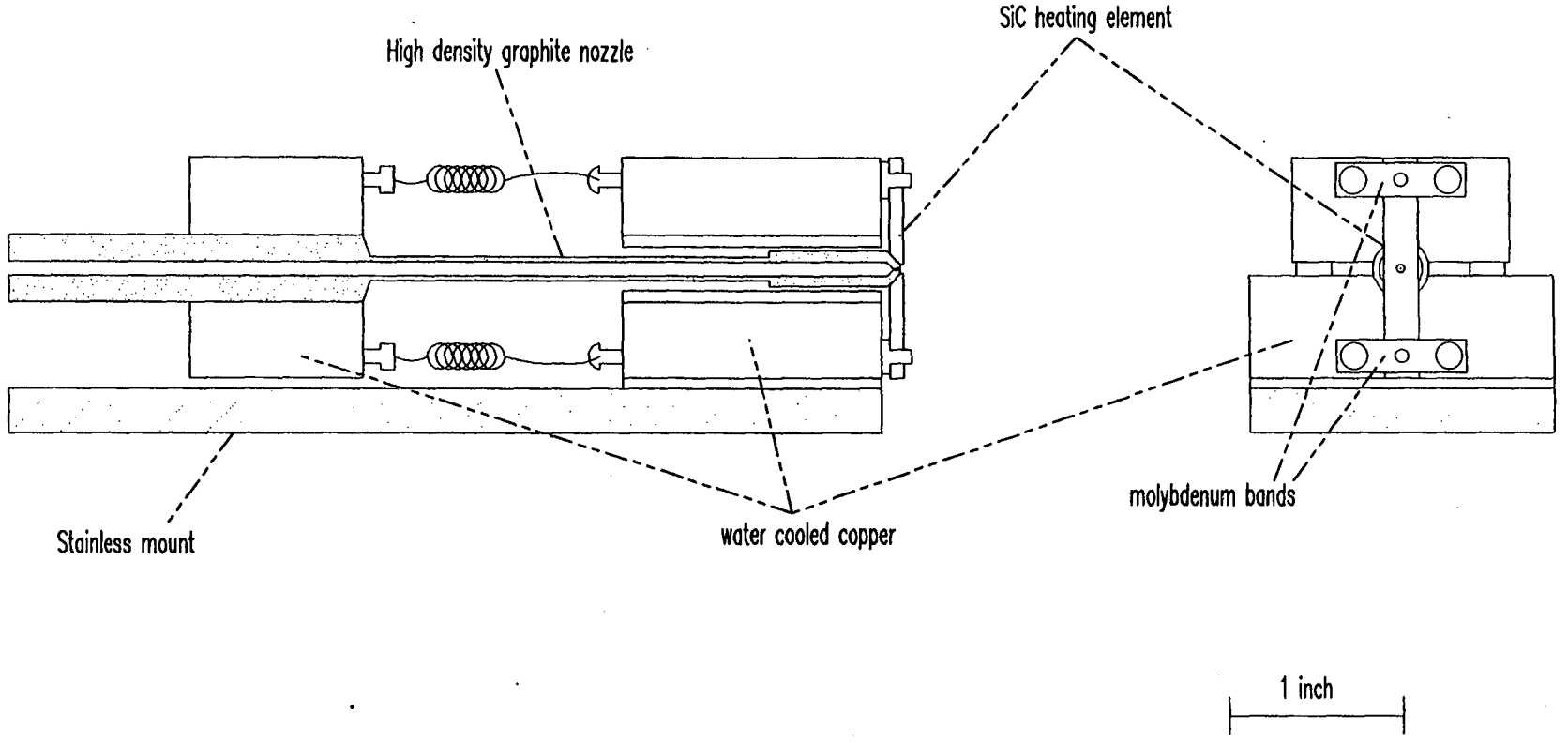

figure 1

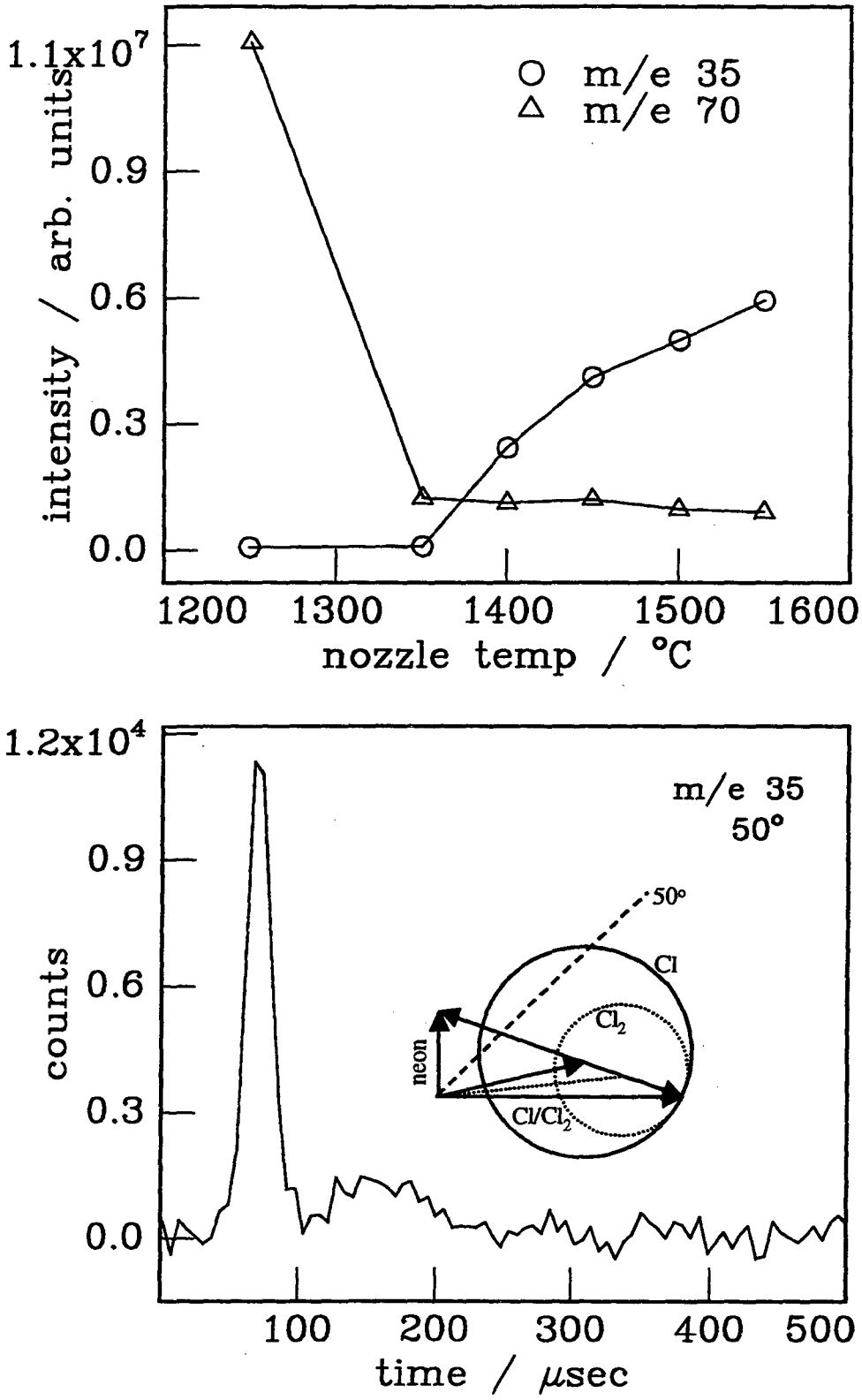
1.1x10^7
0.9
0.6
0.3
0.0
intensity / arb. units
m/e 35
m/e 70
1200
1300
1400
1500
1600
nozzle temp / °C
1.2x10^4
0.9
0.6
0.3
0.0
counts
m/e 35
50°
50°
Cl
Cl2
neon
Cl/Cl2
100
200
300
400
500
time / μsec

figure 2

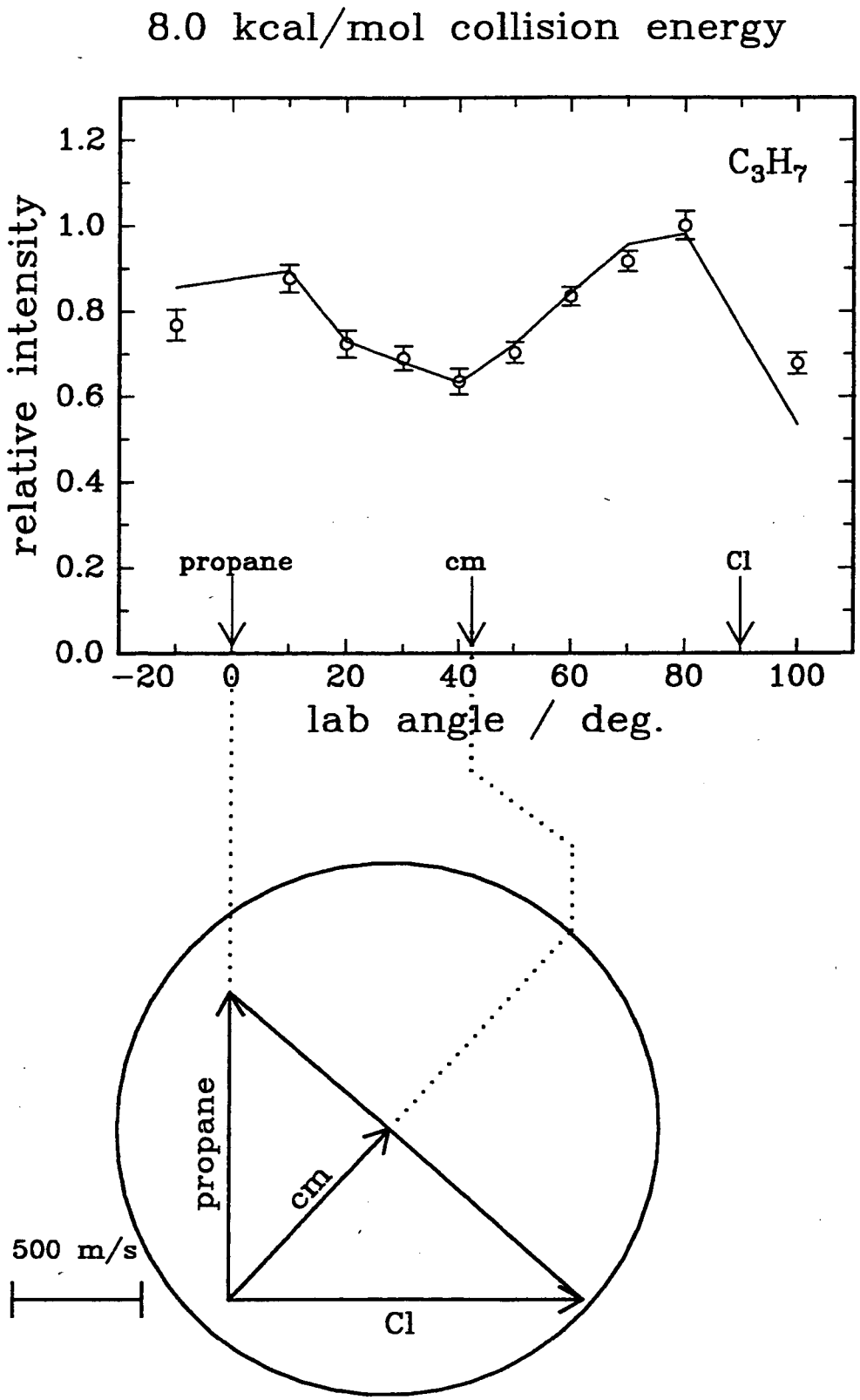
8.0 kcal/mol collision energy
relative intensity
1.2
1.0
0.8
0.6
0.4
0.2
0.0
C_3H_7
propane
cm
Cl
−20
0
20
40
60
80
100
lab angle / deg.
propane
cm
500 m/s
Cl

figure 3

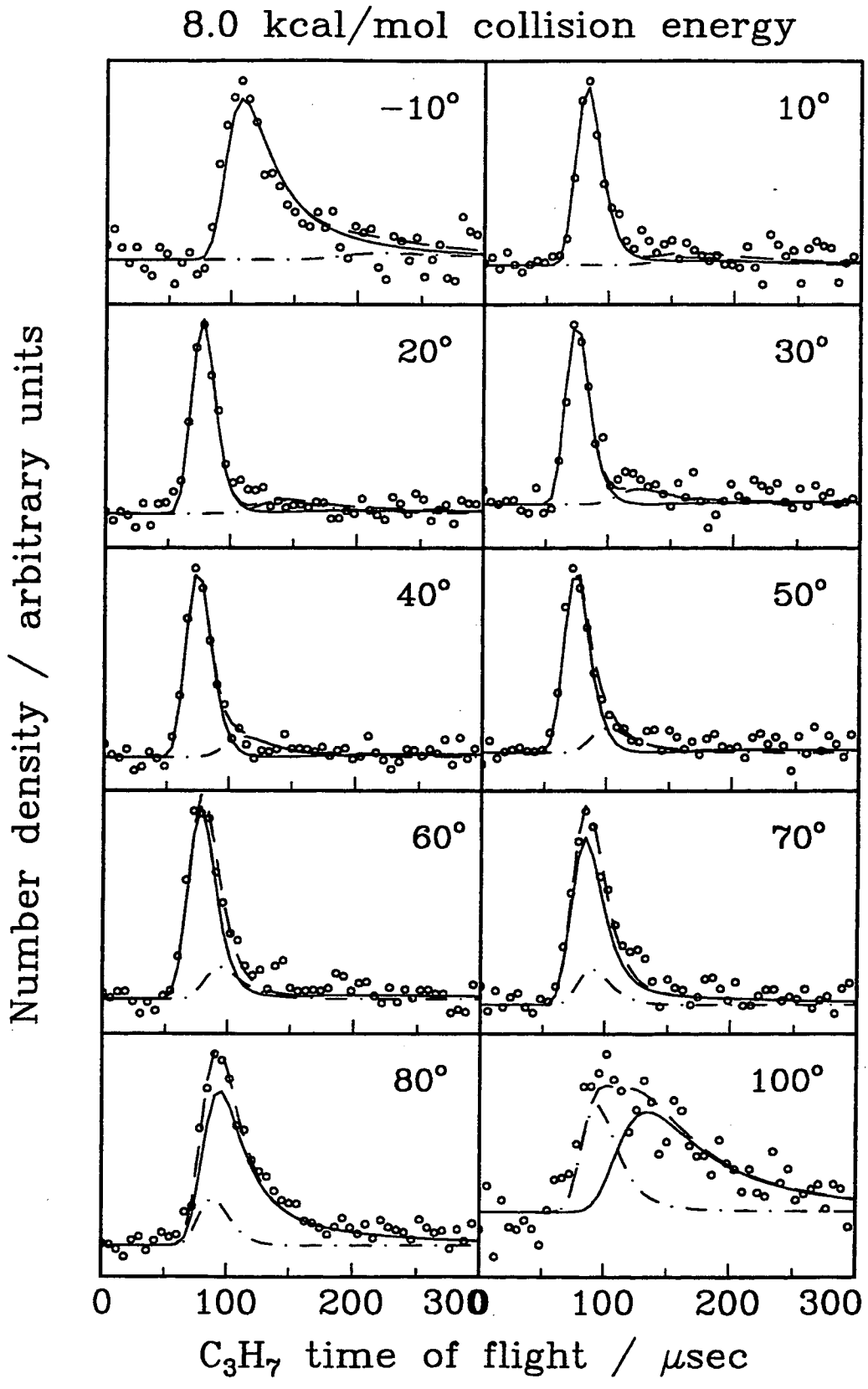
8.0 kcal/mol collision energy
−10°
10°
20°
30°
40°
50°
60°
70°
80°
100°
Number density / arbitrary units
0
100
200
300
100
200
300
C3H7 time of flight / μsec

figure 4

8.0 kcal/mol collision energy

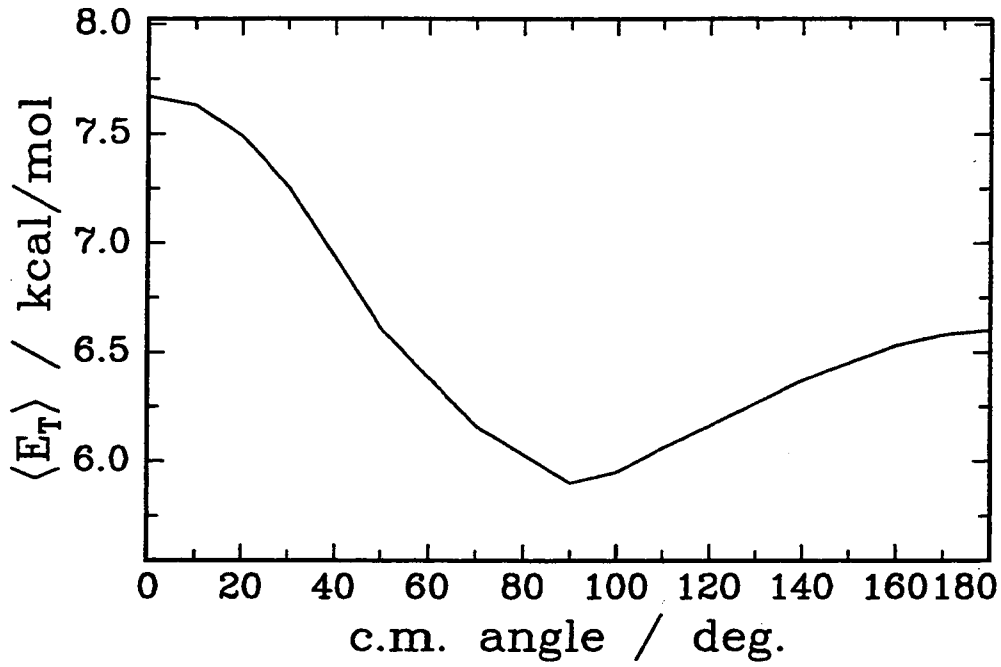

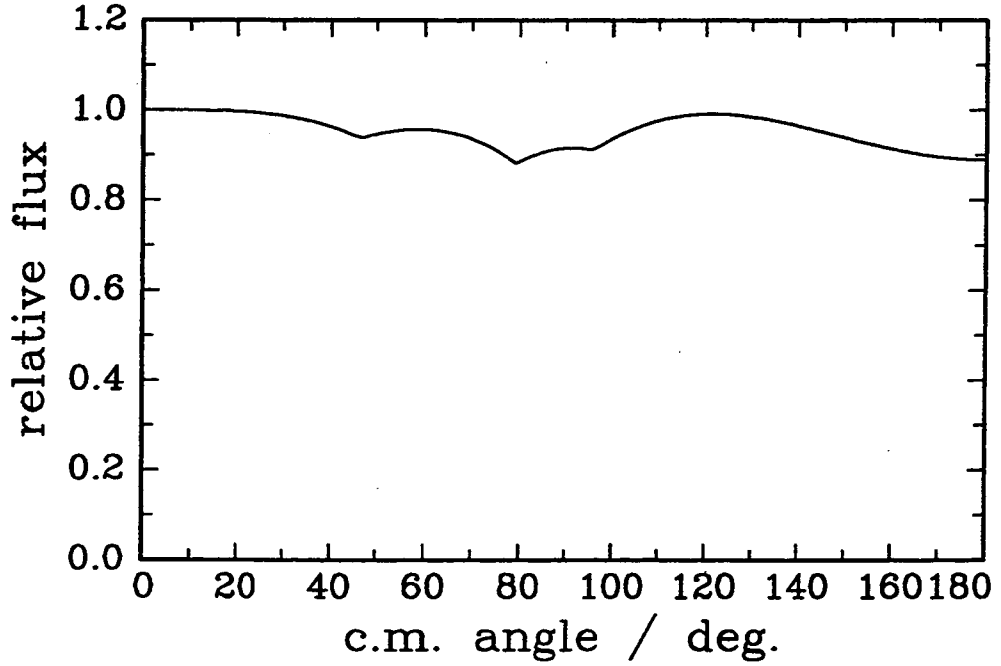

figure 5

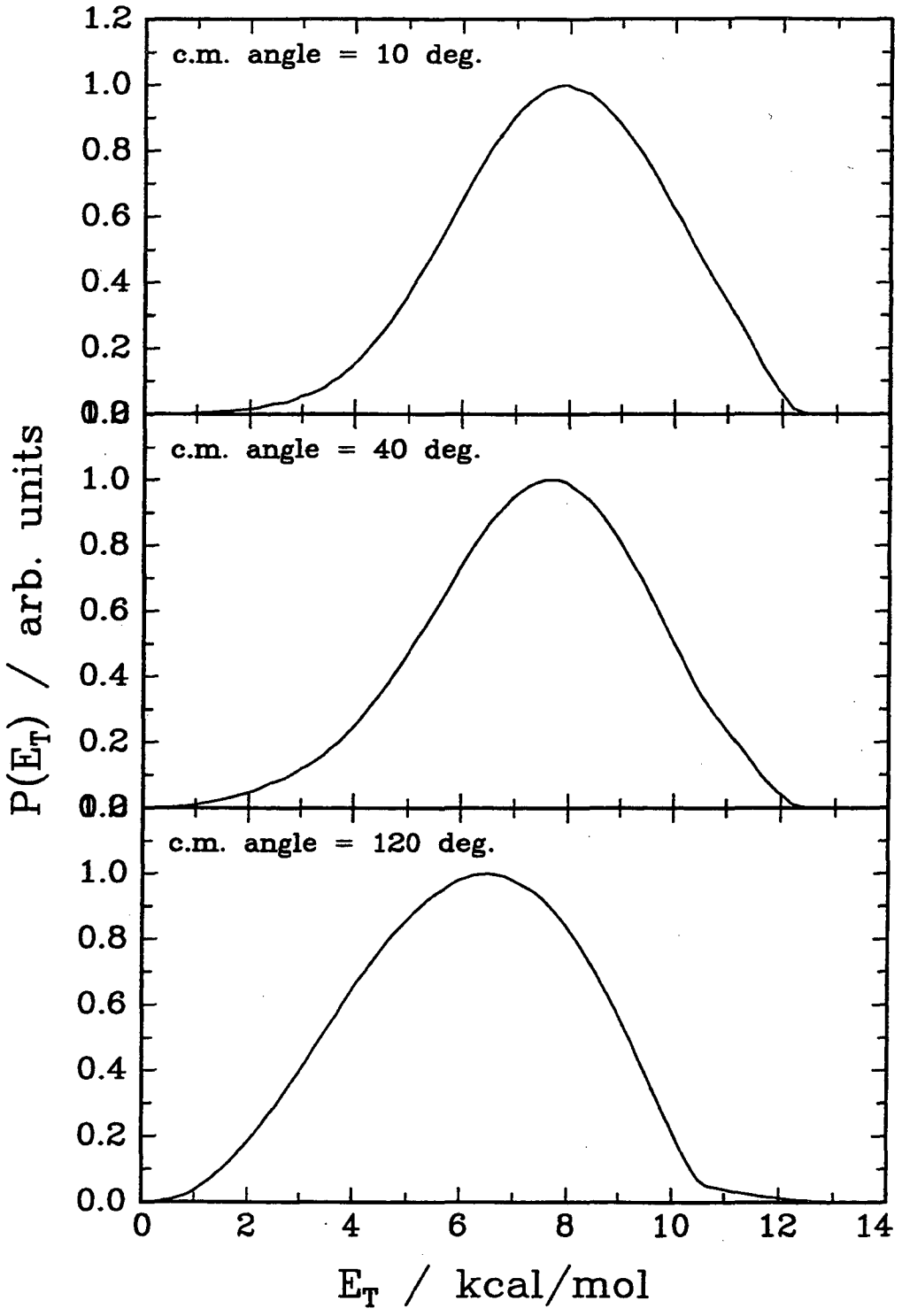
8.0 kcal/mol collision energy
c.m. angle = 10 deg.
c.m. angle = 40 deg.
c.m. angle = 120 deg.
P(E_T) / arb. units
E_T / kcal/mol
0.0
0.2
0.4
0.6
0.8
1.0
1.2
0
2
4
6
8
10
12
14

figure 6

8.0 kcal/mol collision energy

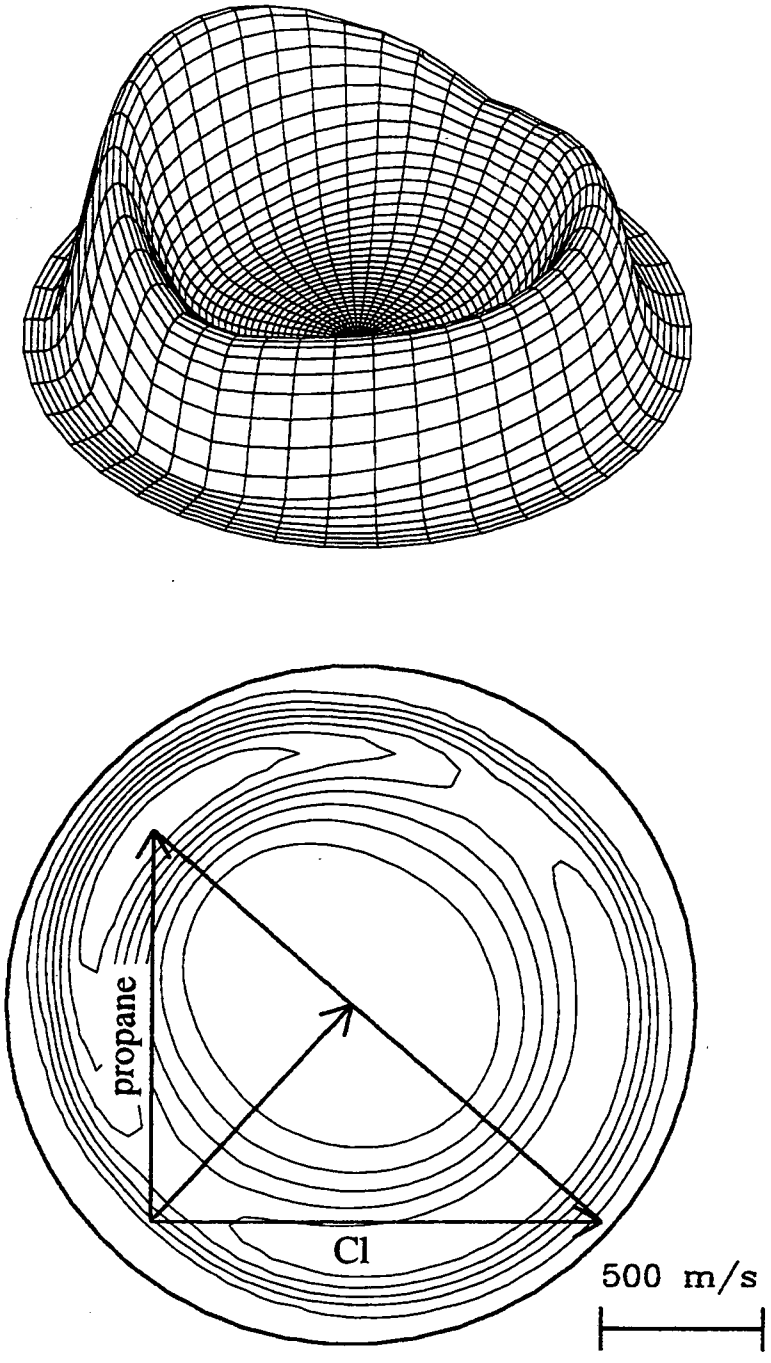

figure 7

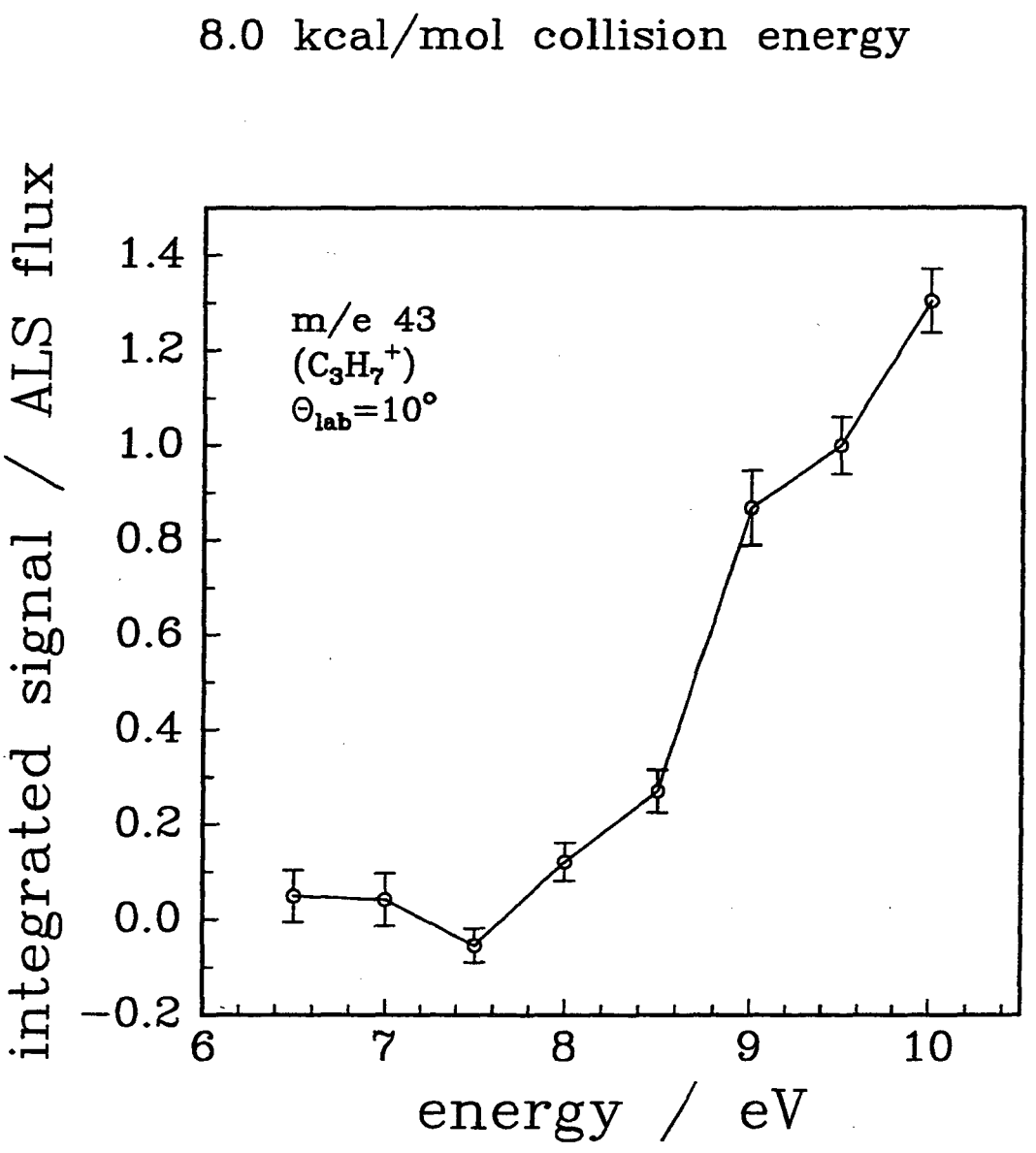
8.0 kcal/mol collision energy
integrated signal / ALS flux
1.4
1.2
1.0
0.8
0.6
0.4
0.2
0.0
−0.2
m/e 43
($C_3H_7^+$)
Θ_{lab}=10°
6
7
8
9
10
energy / eV

figure 8

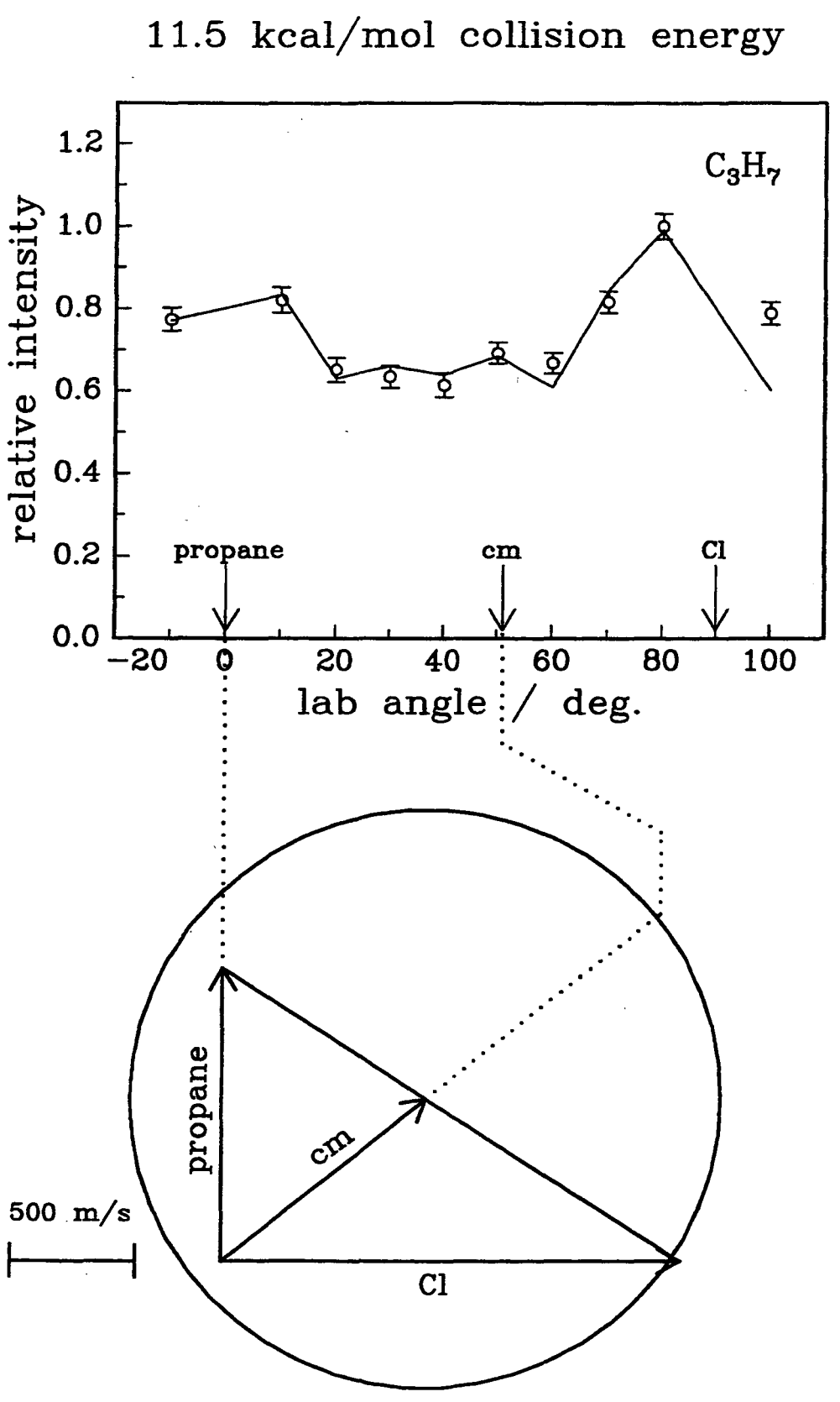
11.5 kcal/mol collision energy
relative intensity
1.2
1.0
0.8
0.6
0.4
0.2
0.0
C_3H_7
propane
cm
Cl
−20
0
20
40
60
80
100
lab angle / deg.
propane
cm
Cl
500 m/s

figure 9

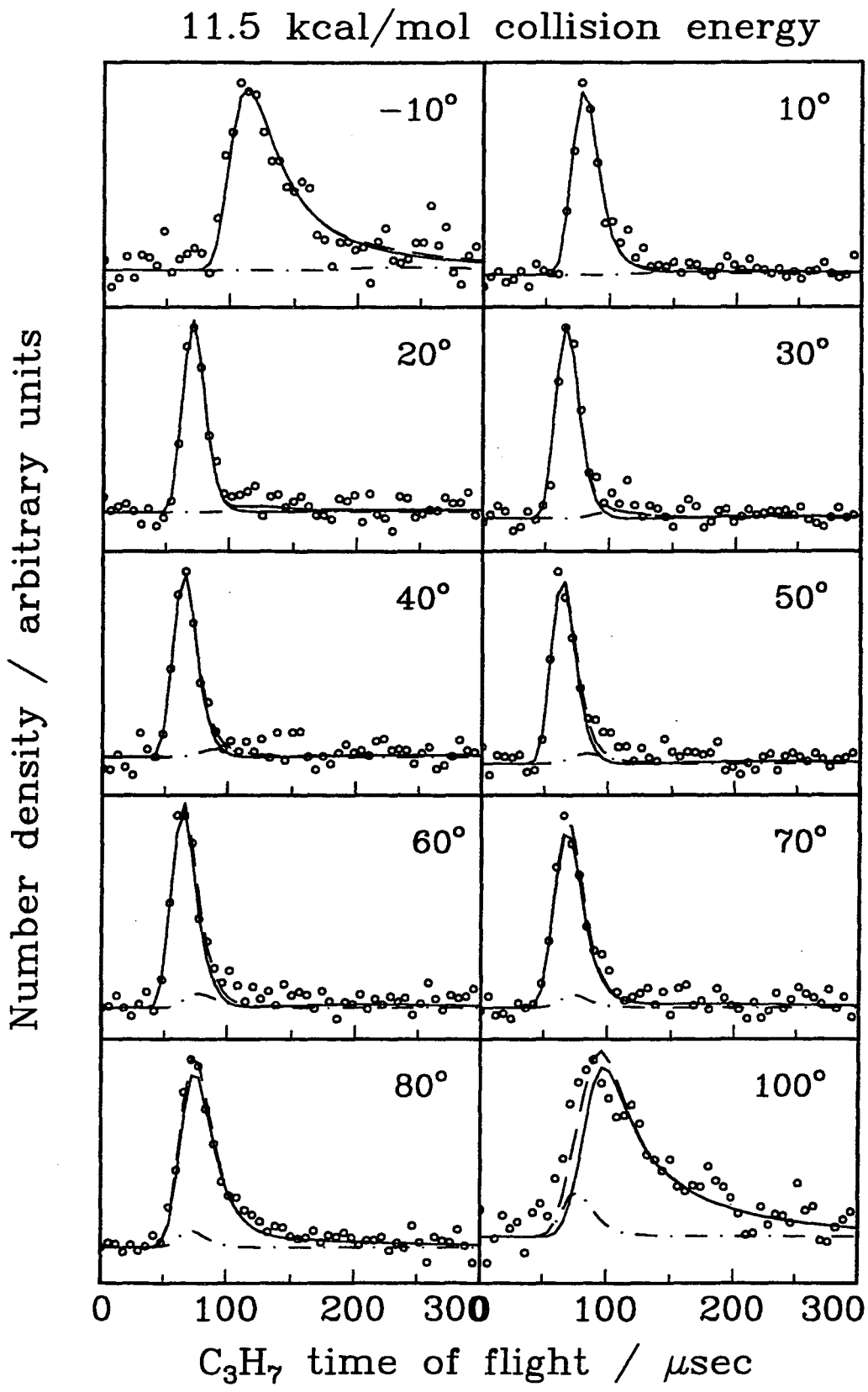
11.5 kcal/mol collision energy
−10°
10°
20°
30°
40°
50°
60°
70°
80°
100°
Number density / arbitrary units
0
100
200
300
100
200
300
C_3H_7 time of flight / μsec

figure 10

11.5 kcal/mol collision energy

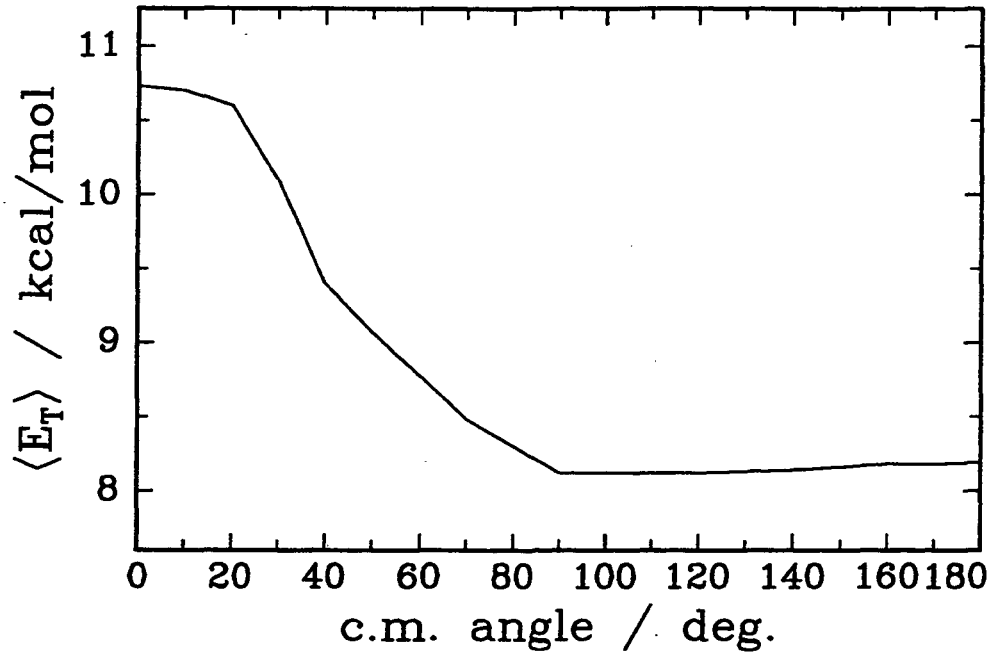

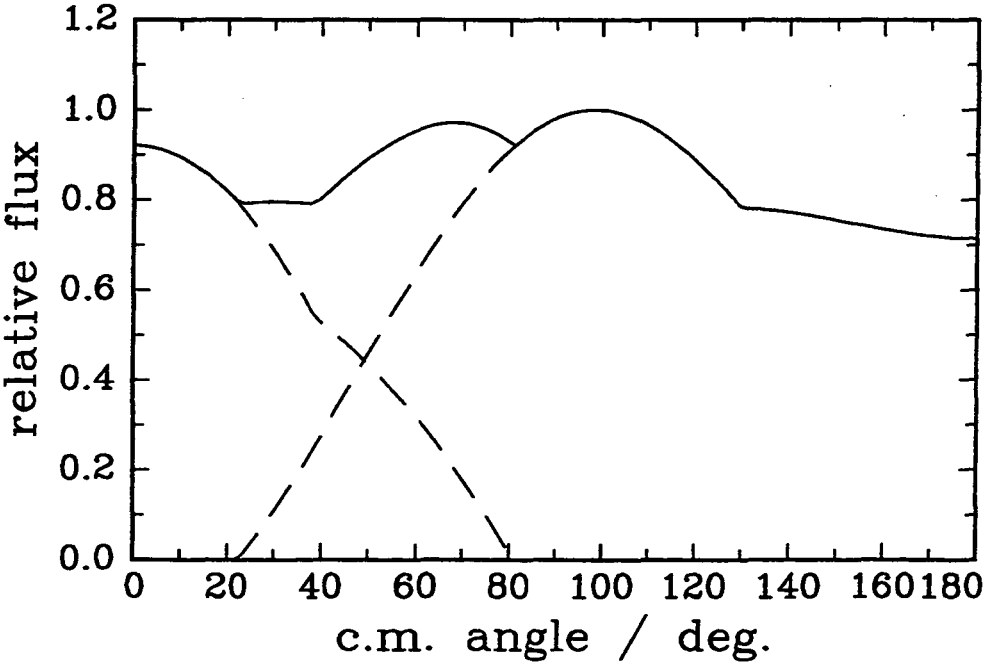

figure 11

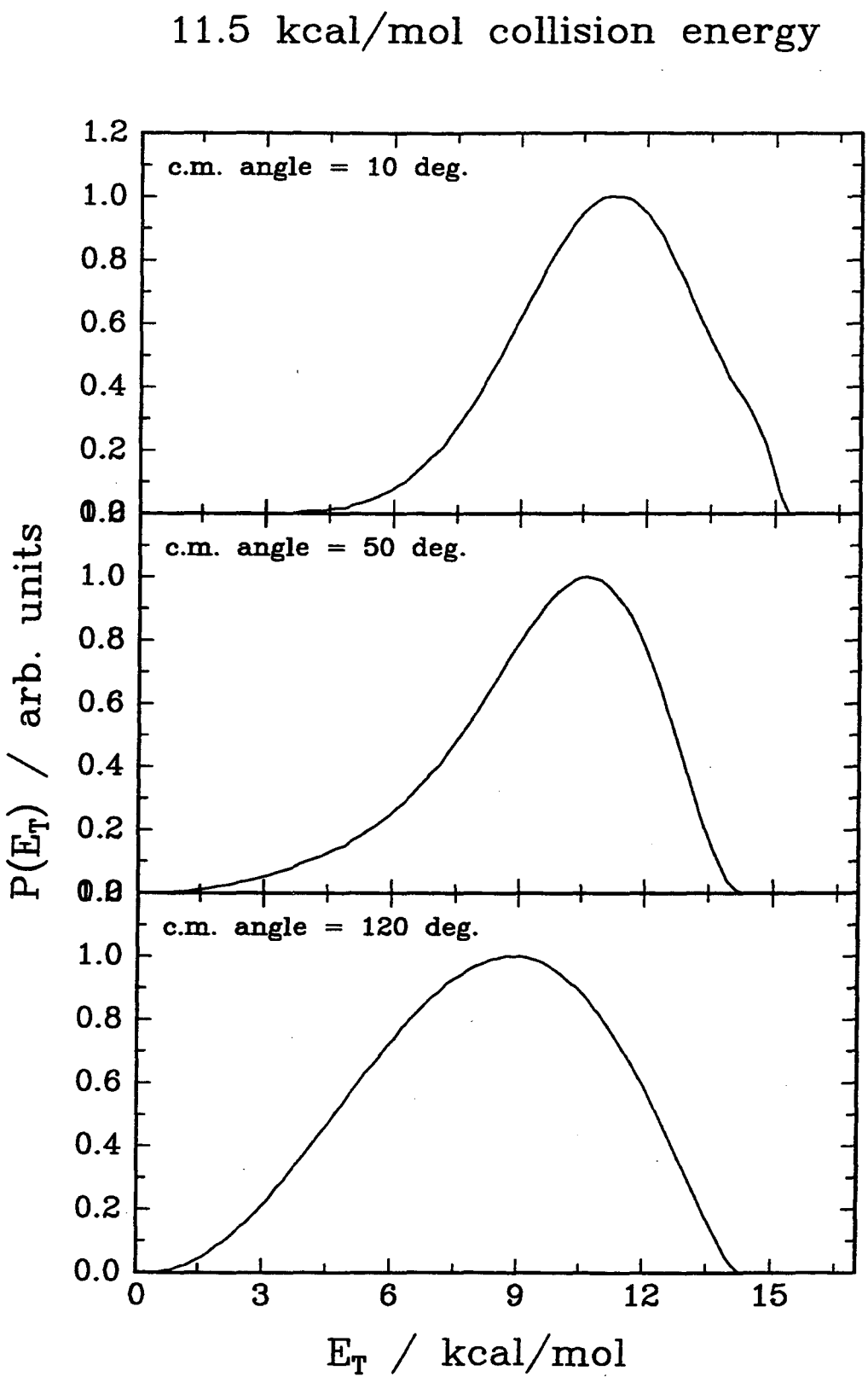
11.5 kcal/mol collision energy
c.m. angle = 10 deg.
c.m. angle = 50 deg.
c.m. angle = 120 deg.
P(E_T) / arb. units
E_T / kcal/mol
0.0
0.2
0.4
0.6
0.8
1.0
1.2
0
3
6
9
12
15

figure 12

11.5 kcal/mol collision energy

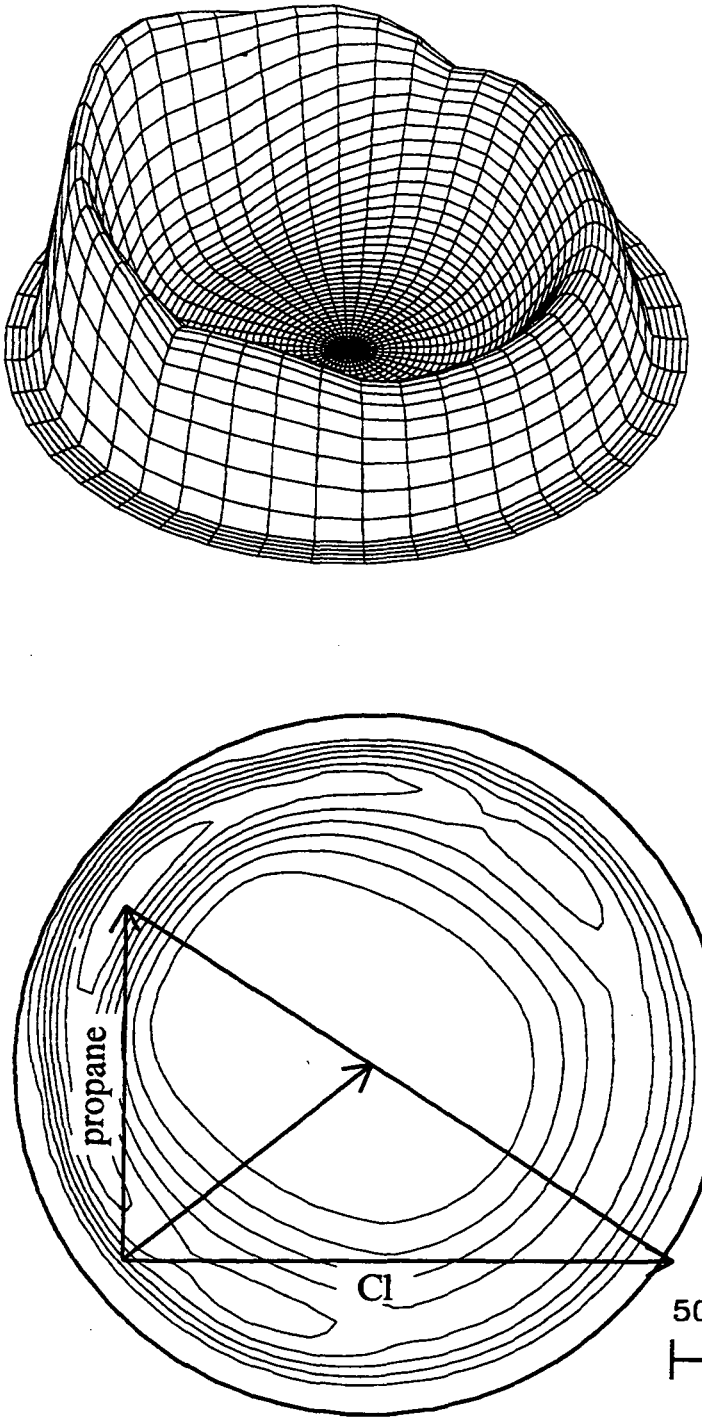

figure 13

11.5 kcal/mol collision energy

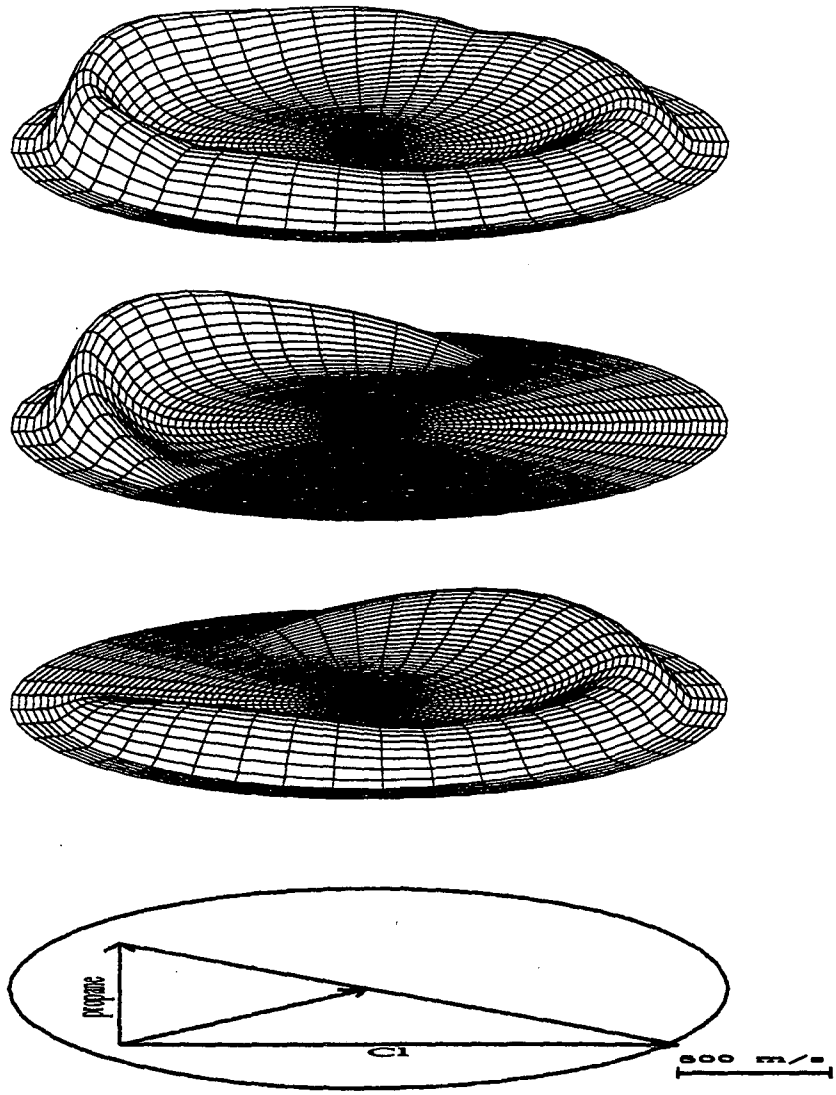

figure 14

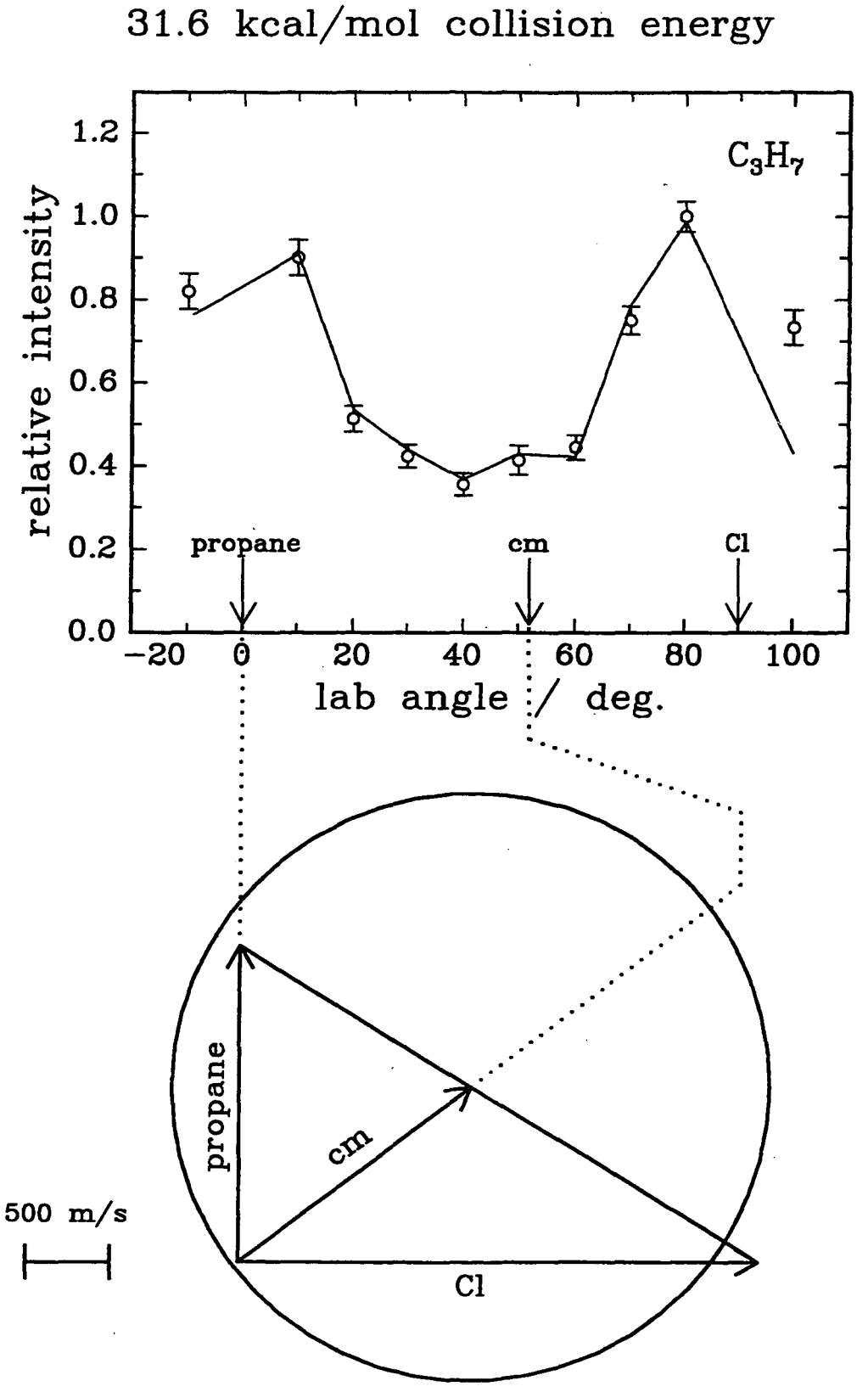
31.6 kcal/mol collision energy
relative intensity
1.2
1.0
0.8
0.6
0.4
0.2
0.0
C_3H_7
propane
cm
Cl
−20
0
20
40
60
80
100
lab angle / deg.
propane
cm
Cl
500 m/s

figure 15

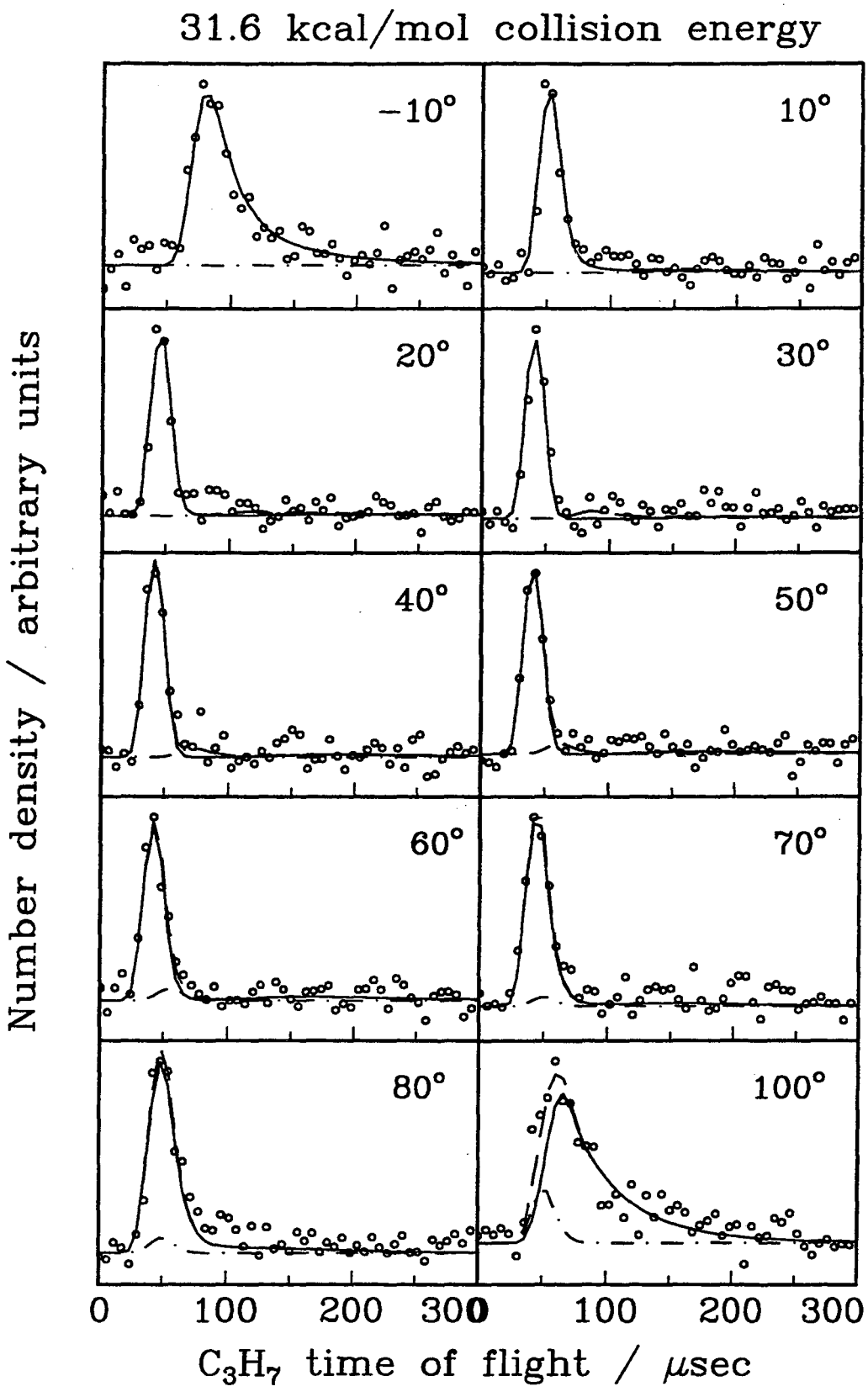
31.6 kcal/mol collision energy
−10°
10°
20°
30°
40°
50°
60°
70°
80°
100°
Number density / arbitrary units
0
100
200
300
100
200
300
C3H7 time of flight / μsec

figure 16

31.6 kcal/mol collision energy

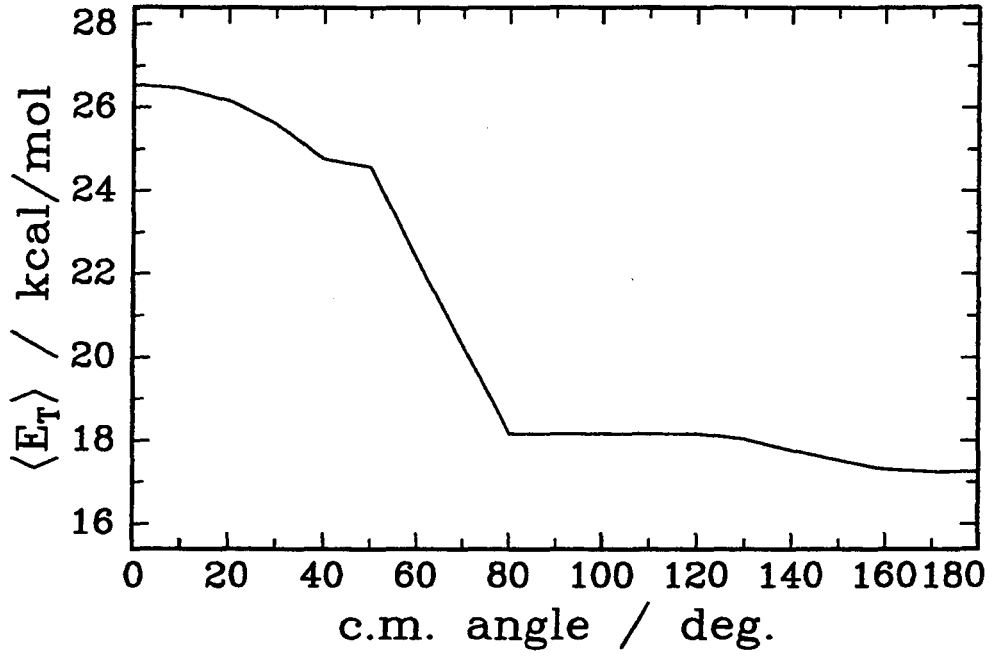

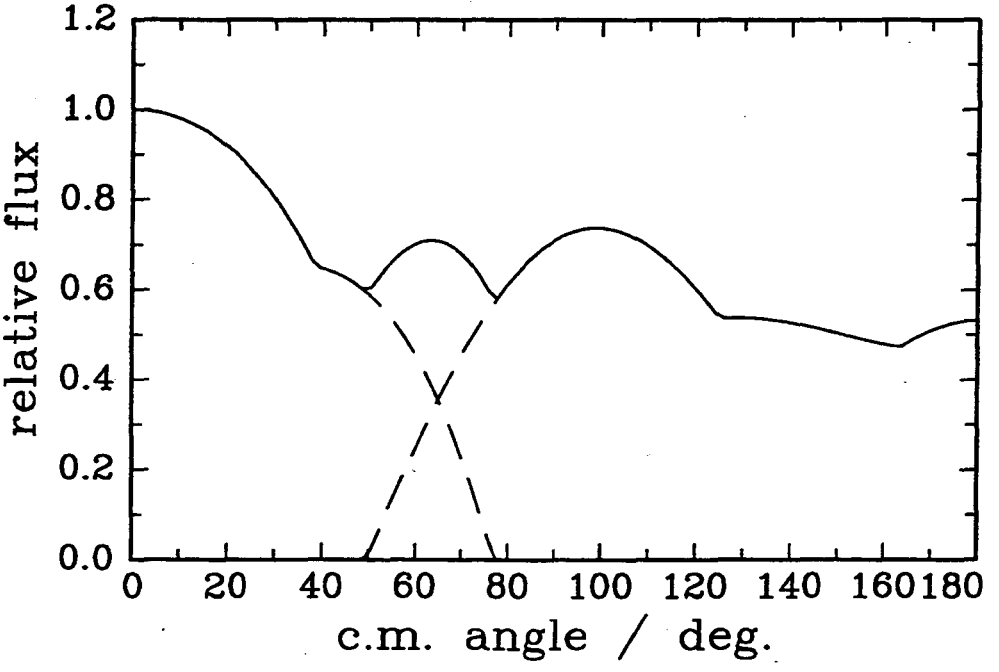

figure 17

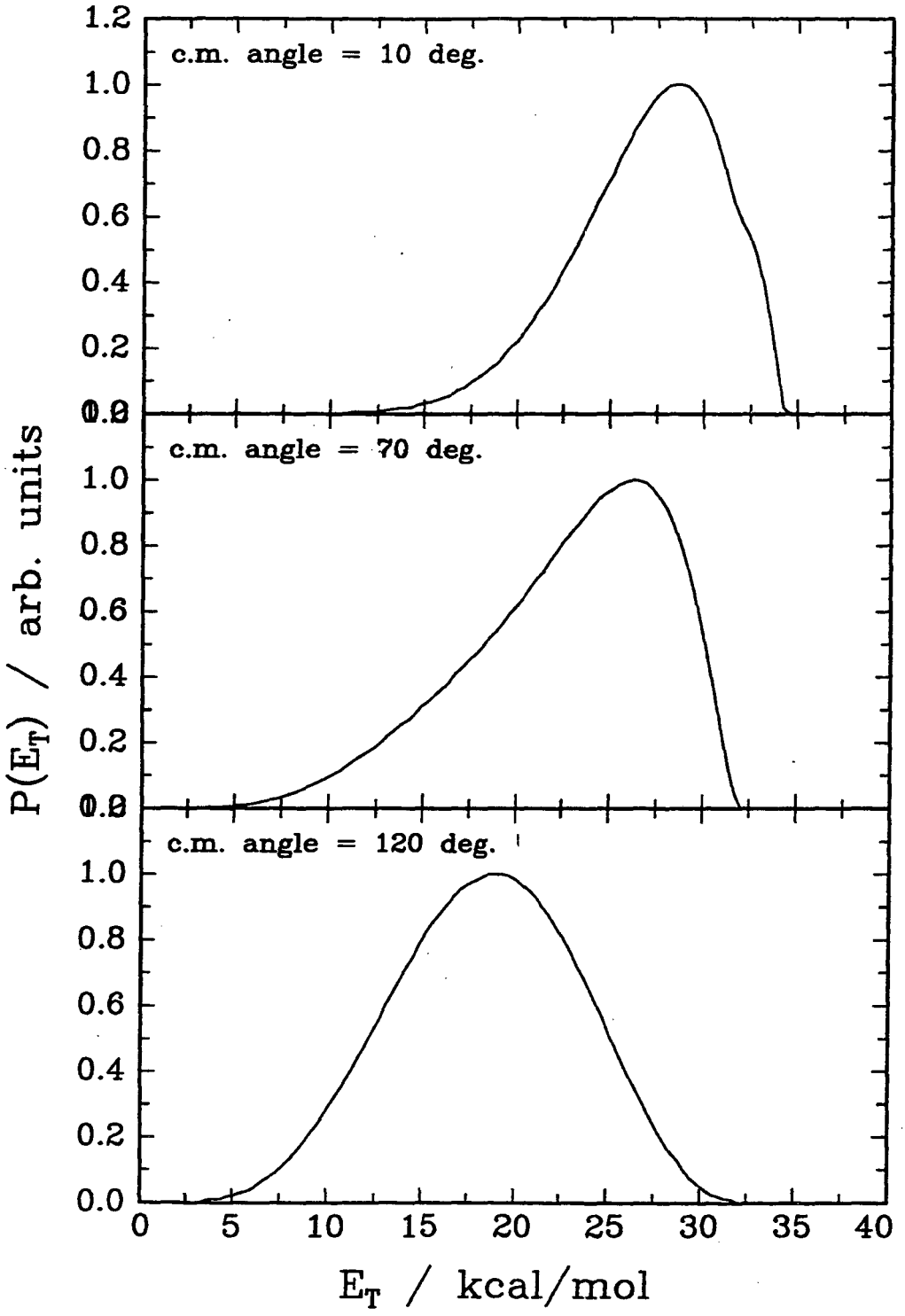
31.6 kcal/mol collision energy
c.m. angle = 10 deg.
c.m. angle = 70 deg.
c.m. angle = 120 deg.
P(E_T) / arb. units
E_T / kcal/mol
0.0
0.2
0.4
0.6
0.8
1.0
1.2
0
5
10
15
20
25
30
35
40

figure 18

31.6 kcal/mol collision energy

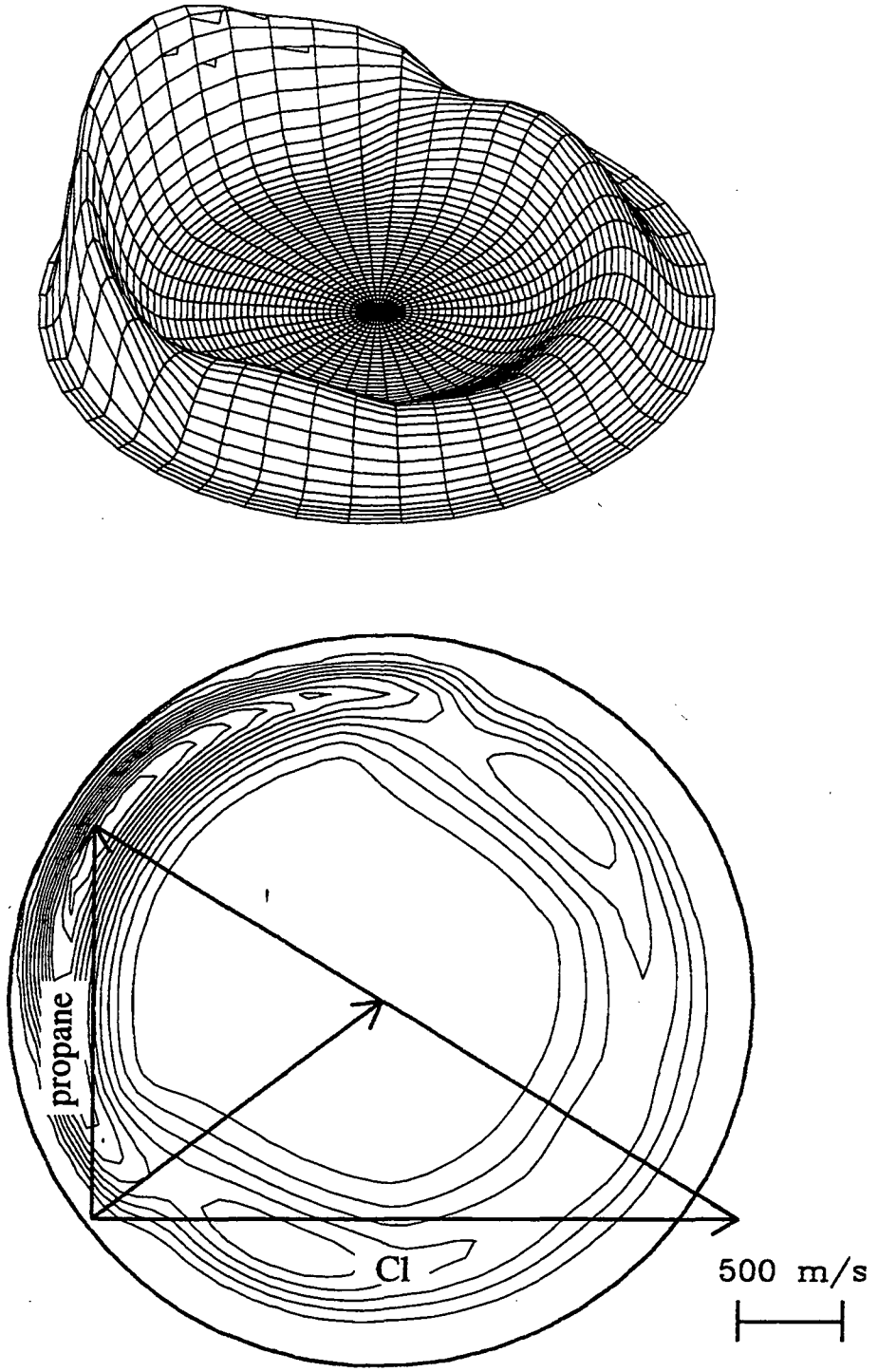

figure 19

31.6 kcal/mol collision energy

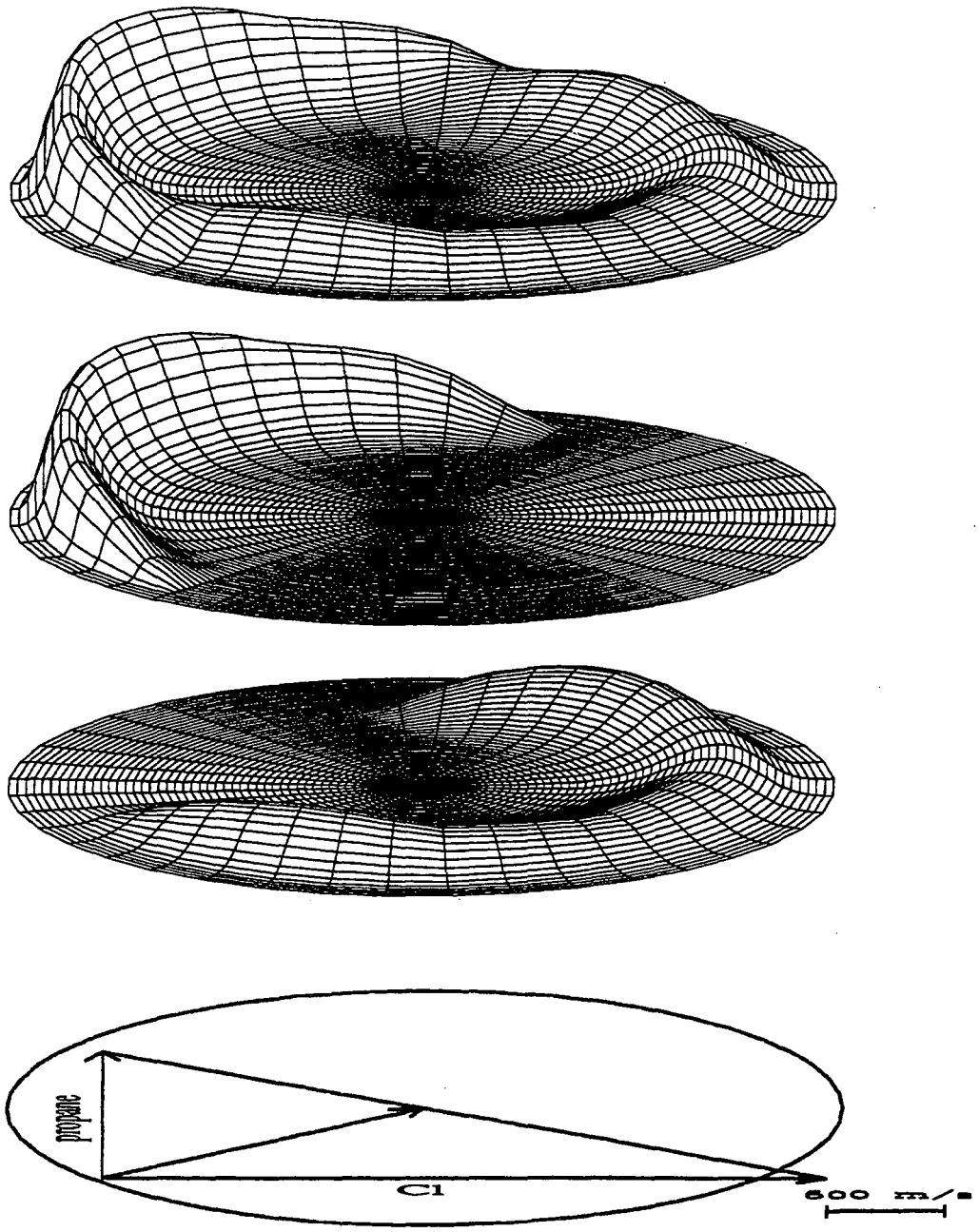

figure 20

Ernest Orlando Lawrence Berkeley National Laboratory
One Cyclotron Road | Berkeley, California 94720

Prepared for the U.S. Department of Energy under Contract No. DE-AC03-76SF00098